The Aeronautical Journal (2023), **127**, pp. 1968–1992
doi:10.1017/aer.2023.23

REGULAR PAPER

Distributed fixed-time control for six-degree-of-freedom spacecraft formation with event-triggered observer

J. Zhang[1], H. Xia[1,*] and Z. Li[2]

[1]Space Control and Inertial Technology Research Center, School of Astronautics, Harbin Institute of Technology, Harbin, China and [2]Shanghai Aerospace Control Technology Institute, Shanghai Academy of Spaceflight Technology, Shanghai, China
*Corresponding author. Email: hxia@hit.edu.cn

Received: 17 September 2022; **Revised:** 21 February 2023; **Accepted:** 23 February 2023

Keywords: 6-DOF leader-following spacecraft formation; Event-triggered fixed-time observer; Fixed-time control; Actuator saturation and input quantisation

Abstract

The paper addresses the six-degree-of-freedom coupled control problem for spacecraft formation flying subject to actuator saturation and input quantisation whilst considering limited communication resources. Firstly, a novel event-triggered distributed observer without continuous communications is presented to recover the information of the virtual leader. Remarkably, by embedding a hyperbolic tangent function-based nonlinear term into the triggering condition, the event-based observer realises a more reasonable trigger threshold. Subsequently, an adding-a-power-integrator-based fixed-time control algorithm is proposed for the follower spacecraft. Further, the control scheme ingeniously compensates for the actuator saturation and the input quantisation problems without embedding auxiliary systems. Finally, numerical simulations are carried out to highlight the advantages of the theoretical results.

Nomenclature

$\boldsymbol{x}_i$	ith follower spacecraft's position states vector
$\boldsymbol{v}_i$	ith follower spacecraft's velocity states vector
$\boldsymbol{u}_i$	ith follower spacecraft's control inputs vector
δ, u_{min}	quantiser parameters
$\boldsymbol{\chi}_s$	decomposition matrix of the actuator saturation
$\boldsymbol{\chi}_q$	decomposition matrix of the input quantisation
χ_{min}	lower bound for elements in the decomposition matrix $\boldsymbol{\chi}_s$
$\boldsymbol{x}_0$	the virtual leader's position states vector
$\boldsymbol{v}_0$	the virtual leader's velocity states vector
$\hat{\boldsymbol{v}}_{i,0}$	the ith follower spacecraft's estimation of $\boldsymbol{v}_0$
$\tilde{\boldsymbol{v}}_{i,0}$	estimation error for the ith follower spacecraft, $\tilde{\boldsymbol{v}}_{i,0} = \hat{\boldsymbol{v}}_{i,0} - \boldsymbol{v}_0$
$\boldsymbol{H}$	the communication topology matrix of the formation
$\boldsymbol{\zeta}_i$	the auxiliary variable related to the observational errors
α, β	fixed-time parameters
o_1, o_2, o_3, o_4	observer gains
$k_{o1}, k_{o2}, k_{o3}, \iota$	parameters of the event-trigger mechanism
B_3	the upper bound of $\|\ddot{\boldsymbol{x}}_0\|$
$\boldsymbol{\Delta}_{i,0}$	the ith follower spacecraft's expected deviation formation vector
$\boldsymbol{e}_{xi}$	tracking errors for ith follower spacecraft, $\boldsymbol{e}_{xi} = \boldsymbol{x}_i - \boldsymbol{\Delta}_{i,0} - \boldsymbol{x}_0$
$\boldsymbol{e}_{vi}$	ith follower spacecraft's tracking errors derivative, $\boldsymbol{e}_{vi} = \boldsymbol{v}_i - \dot{\boldsymbol{\Delta}}_{i,0} - \boldsymbol{v}_0$
$\boldsymbol{\sigma}_i, \boldsymbol{\gamma}_i, \boldsymbol{\gamma}_{di}, \boldsymbol{\kappa}_i$	the auxiliary variable related to the tracking errors
k_1, k_2, k_3, k_4, k_5	controller gains

Abbreviations

SFF	spacecraft formation flying
ETM	event-trigger mechanism
ASKAE	attitude station keeping absolute error
PSKAE	position station keeping absolute error

1.0 Introduction

The spacecraft formation flying (SFF) system has drawn extensive attention owing to its costs, robustness and flexibility [1] in recent years, which can overcome the limitations of using a single spacecraft for mission goal accomplishment. Numerous space missions by deploying SFF system such as monitoring [2], remote sensing [3], and on-orbit services [4] have been successfully launched.

For the SFF tracking control problem, the convergence rate is an important performance indicator reflecting the proposed algorithm's effectiveness. Most of the existing studies [5, 6] achieve asymptotic stability results only, of which convergence time tends to infinity. In contrast to the asymptotic control algorithm, the finite-time control algorithm can provide faster convergence rate, higher precision, and better robustness, with the adding a power integrator technique [7] the terminal sliding mode theorem [8], and the homogeneity theorem [9] as the primary design methods. However, the prior estimation of the finite-time control algorithm's convergence time is decided by the initial states. As an extension of finite-time method, the fixed-time control algorithm was introduced in [10], where the settling time is uniformly bounded with regard to the initial states. One of the basic synchronisation algorithms for the formation keeping and reconstruction problem is leader-follower formation, where the leader runs in a predetermined trajectory while the followers need coordinate. Following the above frameworks, Ren first proposed an SFF control algorithm [11] considering the two cases of whether all follower spacecraft can access the reference trajectory. In light of this, Gao proposed a fixed-time coordinated algorithm for the SFF system [12]. However, most scholars concentrated their research on the attitude coordinated control or modeled the translational and rotational motions separately, ignoring the mutual coupling between the orbit and attitude.

In practice, continuous interactive communication of formation spacecraft is challenging due to the limitation of onboard resources, especially communication channel bandwidth. To this end, the seminal work [13, 14] reported an event-triggered method premised on asynchronous, aperiodic communication. Thereafter, the event-based control has drawn considerable attentions [15–20] (just to name a few). In particular, Nowzari provides a comprehensive account of the motivation behind applying event-triggered strategies in multi-agent systems [15]. Further, continuous communication can be avoided both in the fixed-time controller algorithm update and in the triggering condition monitoring in [17]. Despite this, it is worth noting that the lower limit of the trigger threshold for most existing works has a stable value, whether in the transient or steady state of the system. In other words, the lower limit of the trigger threshold does not increase when the error is large; on the contrary, the lower limit does not decrease when the error is small, which results in a waste of communication resources. Bearing this in mind, by utilising the characteristics of the hyperbolic tangent function, the change of the lower limit of the trigger threshold with the error is discussed in [20]. Nevertheless, it is noticed that the event-trigger mechanism (ETM) in [20] depends on continuous communications. As such, how to design an ETM for multiple spacecraft systems, which has a more flexible trigger threshold lower limit and eliminates continuous communication, still remains open and awaits a breakthrough.

Another practical problem for spacecraft is that the onboard actuators are susceptible to suffering from quantisation errors and magnitude constraints. Data transmission between the attitude control module and actuator module would introduce input quantisation errors, which may lead to the degradation of the control performance. To alleviate this concern, control algorithms that take account of input quantisation were investigated for spacecraft systems. In [21] and [22], the functional relationship between the control input and the quantised input is established by the non-linear decomposition of the quantised signal. Suffering from the piece-wise quantised input, most relevant literatures have used the above

https://doi.org/10.1017/aer.2023.23 Published online by Cambridge University Press

or similar methods to overcome the technique difficulty. Additionally, actuators have saturation constraints due to physical structure and energy limitations, which will severely limit the performance of the closed-loop system if the actuator is always saturated. Various methods have been designed for the input saturation problem, such as adding a neural network-based compensator [23], introducing an auxiliary system [12], constructing a command prefilter [24], and so on. However, the above methods of dealing with actuator saturation dramatically increased the complexity of the control algorithm. Although scholars have extensively studied the input quantisation and actuator saturation problem, nearly no research has addressed the fixed-time anti-saturation and anti-quantisation control problem for 6-DOF SFF.

Statistically, most SFF missions are carried out by small spacecraft operating in low Earth orbit (LEO) with a mass of less than 500kg [25]. The light mass of the spacecraft means limited onboard resources, such as communication bandwidth, actuator capability, and energy. Given these onboard resource constraints, it is worth investigating the design of a distributed controller to meet the demands of increasingly complicated SFF missions for the spacecraft's rapid and precise manoeuver capabilities. In this paper, we consider the onboard resource constraints for the problem of limited communication resources, actuator saturation, and input quantisation. Here, limited communication resources implies that only a portion of the spacecraft can access the virtual leader. Besides, for SFF operating in LEO, simultaneous attitude and constellation control are essential for timely identification and counteracting time-critical orbit spacing violations. In other words, designing a six-degree-of-freedom controller for the SFF mission that considers the attitude-orbit coupling is necessary. Bearing the discussion above in mind, we address the attitude and position coupled tracking fixed-time control problem for SFF systems considering limited communication resources, actuator saturation and input quantisation. A distributed event-triggered observer is first proposed to recover the virtual leader's velocity states. More importantly, the event-based observer realises a more reasonable trigger threshold and less communication resource usage by embedding a hyperbolic tangent function-based nonlinear term into the triggering condition. Subsequently, a fixed-time distributed control algorithm is developed for the SFF system, handling the actuator saturation and the input quantisation problems ingeniously without embedding auxiliary systems. The main contributions of this paper are summarised as follows.

(1) A novel distributed event-based fixed-time observer is developed to estimate the states of the virtual leader for SFF system. Compared with the traditional observer presented in [12], the observer proposed in this paper alleviate the chattering caused by symbolic functions. Besides, an additional nonlinear term is adopted by the observer to guarantee the asymptotic stability of the whole closed-loop system.

(2) Compared with the existing ETM in [17], the ETM of the observer proposed in this paper realises a more reasonable trigger threshold and a lower bound of trigger threshold with characteristics of the exponential function and the hyperbolic tangent function in the transient and steady state.

(3) A distributed fixed-time attitude control scheme is established in the presence of the actuator saturation and the input quantisation problems by utilising the adding a power integrator technique. In contrast to the existing methods in [26], the proposed control scheme compensates the actuator saturation and the input quantisation problems ingeniously without embedding auxiliary systems.

The remainder of this paper is as follows. Section II introduces some preliminaries. The observer-based distributed control scheme is provided in Section III. Section IV offers numerical simulations. Finally, Section V gives a conclusion.

2.0 Preliminaries

2.1 Notations and lemmas

Define $\|\cdot\|$ as the induced norm of a matrix or the Euclidean norm of a vector. $\boldsymbol{I}_n$ denotes the $n \times n$ identity matrix. $\otimes$ is defined as the Kronecker product. $\lambda_{\min}(\cdot)$ and $\lambda_{\max}(\cdot)$ represent

https://doi.org/10.1017/aer.2023.23 Published online by Cambridge University Press

the minimum and maximum eigenvalues of a symmetric matrix. The basic operations of the dual number, quaternion and dual quaternion are defined in the appendix. Given a vector $\boldsymbol{x} = [x_1, x_2, \ldots, x_n]^{\mathrm{T}} \in \mathbb{R}^n$ and $\alpha > 0$, we denote $\mathrm{sig}^{\alpha}(\boldsymbol{x}) = \left[\mathrm{sign}(x_1)\,|x_1|^{\alpha}, \mathrm{sign}(x_2)\,|x_2|^{\alpha}, \ldots, \mathrm{sign}(x_n)\,|x_n|^{\alpha}\right]^{\mathrm{T}}$ and $|\boldsymbol{x}| = [|x_1|, |x_2|, \ldots, |x_n|]^{\mathrm{T}}$, where $\mathrm{sign}(\cdot)$ is the signum function. $\mathrm{diag}(x_1, x_2, \ldots, x_n)$ denotes a block-diagonal matrix. $\max(x_1, x_2, \ldots, x_n)$ and $\min(x_1, x_2, \ldots, x_n)$ denote the maximum and minimum value in $(x_1, x_2, \ldots, x_n)$, respectively.

In order to get the main results of this paper, the following lemmas are introduced.

Lemma 1. [27] *If the time derivative of a Lyapunov function V satisfies $\dot{V} \leq -\kappa_1 V^{\rho_1} - \kappa_2 V^{\rho_2}$ where $\kappa_1 > 0, \kappa_2 > 0, 0 < \rho_1 < 1$, and $\rho_2 > 1$ are some constants, the value of V converges to zero in fixed-time. The settling time satisfies $T \leq 1/[\kappa_1(1-\rho_1)] + 1/[\kappa_2(\rho_2 - 1)]$.*

Lemma 2. [28] *For any $x \in \mathbb{R}, y \in \mathbb{R}$, the inequality $|\mathrm{sig}^{\alpha}(x) - \mathrm{sig}^{\alpha}(y)| \leq 2^{1-\alpha}|x-y|^{\alpha}$ is tenable if $\alpha \in (0, 1]$ holds.*

Lemma 3. [28] *For any $x \in \mathbb{R}, y \in \mathbb{R}$, the following inequality is tenable when $\alpha \geqslant 1$. $|x-y|^{\alpha} \leq 2^{\alpha-1}\,|\mathrm{sig}^{\alpha}(x) - \mathrm{sig}^{\alpha}(y)|$*

Lemma 4. [29] *For any positive constant $a_1, a_2, \cdots, a_n$, the following inequality is tenable if $p \in (0, 2)$ holds. $\left(a_1^2 + a_2^2 + \cdots + a_n^2\right)^p \leq \left(a_1^p + a_2^p + \cdots + a_n^p\right)^2$*

Lemma 5. [30] *For any $x \in \mathbb{R}, y \in \mathbb{R}, c > 0, d > 0, \gamma > 0$, the inequality $|x|^c|y|^d \leq \frac{c\gamma|x|^{c+d}}{c+d} + \frac{d|y|^{c+d}}{\gamma^{c/d}(c+d)}$ is tenable.*

Lemma 6. [12] *For any $x_i \in \mathbb{R}, i = 1, 2, \ldots, n$, the following inequality is tenable if $v \in (0, 1]$. $\left(\sum_{i=1}^n |x_i|\right)^v \leq \sum_{i=1}^n |x_i|^v \leq n^{1-v}\left(\sum_{i=1}^n |x_i|\right)^v$.*

Lemma 7. [9] *For any $x_i \in \mathbb{R}, i = 1, 2, \ldots, n$, the following inequality is tenable if $v > 1$. $\sum_{i=1}^n |x_i|^v \leq \left(\sum_{i=1}^n |x_i|\right)^v \leq n^{v-1}\sum_{i=1}^n |x_i|^v$.*

Lemma 8. [31] *For matrices $\boldsymbol{X}, \boldsymbol{Y}$ with equal dimensions and positive constant η, the following inequality satisfies: $2\boldsymbol{X}^{\mathrm{T}}\boldsymbol{Y} \leq \frac{1}{\eta}\boldsymbol{X}^{\mathrm{T}}\boldsymbol{X} + \eta\boldsymbol{Y}^{\mathrm{T}}\boldsymbol{Y}$.*

2.2 Mathematical model

The coordinate system used in this paper is shown in Fig. 1, which defines the Earth-centred inertial frame $O_E X_I Y_I Z_I$ and the jth spacecraft body frame $O_{Bj} X_{Bj} Y_{Bj} Z_{Bj}$. O_E is the centre of the Earth and O_{Bj} is the centre of mass of the jth deputy.

Based on dual quaternion, the states of ith spacecraft can be described as $\hat{\boldsymbol{q}}_i$ and $\hat{\boldsymbol{\omega}}_i$, where $\hat{\boldsymbol{q}}_i = \boldsymbol{q}_i + \varepsilon\frac{1}{2}\boldsymbol{q}_i \circ \boldsymbol{r}_i$, $\hat{\boldsymbol{\omega}}_i = \boldsymbol{\omega}_i + \varepsilon(\dot{\boldsymbol{r}}_i + \boldsymbol{\omega}_i \times \boldsymbol{r}_i)$, ε is the dual unit that satisfies $\varepsilon^2 = 0, \varepsilon \neq 0$. $\boldsymbol{q}_i$ is the quaternion describing the rotation of the ith spacecraft body frame relative to the inertial frame. $\boldsymbol{r}_i = \left[0, (\vec{\boldsymbol{r}}_i)^{\mathrm{T}}\right]^{\mathrm{T}} \in \mathbb{R}^4$, $\vec{\boldsymbol{r}}_i \in \mathbb{R}^3$ denotes the position of the ith spacecraft expressed in the spacecraft body frame. $\boldsymbol{\omega}_i = \left[0, (\vec{\boldsymbol{\omega}}_i)^{\mathrm{T}}\right]^{\mathrm{T}} \in \mathbb{R}^4$, $\vec{\boldsymbol{\omega}}_i \in \mathbb{R}^3$ is the angular velocity of the ith spacecraft body frame relative to the inertial frame expressed in the body frame. The dynamic equations of six-DOF motion are [32]

$$\dot{\hat{\boldsymbol{q}}}_i = \frac{1}{2}\hat{\boldsymbol{q}}_i \circ \hat{\boldsymbol{\omega}}_i \tag{1}$$

$$\dot{\hat{\boldsymbol{\omega}}}_i = M_i^{-1} * \left\{\hat{\boldsymbol{F}}_{ig} + \boldsymbol{sat}\left[\boldsymbol{Q}\left(\hat{\boldsymbol{F}}_{ic}\right)\right] + \hat{\boldsymbol{F}}_{ip} - \hat{\boldsymbol{\omega}}_i \times \left(\boldsymbol{M}_i * \hat{\boldsymbol{\omega}}_i\right)\right\} \tag{2}$$

where $\hat{\boldsymbol{F}}_{ig} = \boldsymbol{f}_{ig} + \varepsilon\boldsymbol{\tau}_{ig} = -\mu m_i \boldsymbol{r}_i / \|\boldsymbol{r}_i\|^3 + \varepsilon 3\mu \boldsymbol{r}_i \times \left(\overline{\boldsymbol{J}}_i \boldsymbol{r}_i\right) / \|\boldsymbol{r}_i\|^5$ denotes the gravity dual force, $\hat{\boldsymbol{F}}_{ic} = \boldsymbol{f}_{ic} + \varepsilon\boldsymbol{\tau}_{ic}$ denotes the control dual force that is yet to be designed, $\boldsymbol{sat}\left[\boldsymbol{Q}\left(\hat{\boldsymbol{F}}_{ic}\right)\right]$ denotes the control dual force with actuator saturation and input quantisation, $\hat{\boldsymbol{F}}_{ip} = \boldsymbol{f}_{ip} + \varepsilon\boldsymbol{\tau}_{ip}$ denotes the disturbing dual

https://doi.org/10.1017/aer.2023.23 Published online by Cambridge University Press

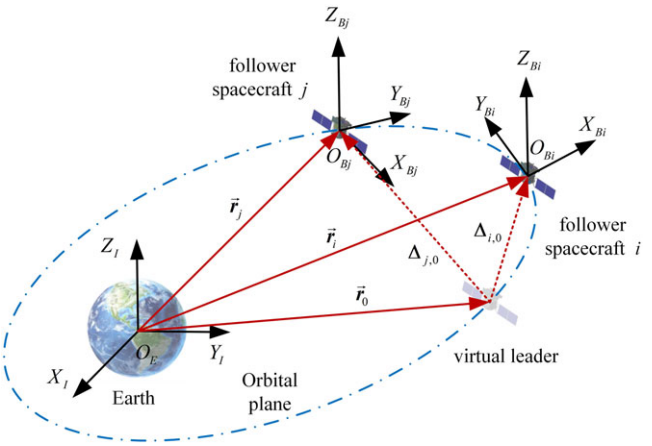

Figure 1. *Coordinate system.*

force. μ is the gravitational parameter of Earth. Define that m_i and $\boldsymbol{J}_i \in \mathbb{R}^{3\times3}$ are the mass and inertia matrix of the ith deputy, respectively. The matrix $\boldsymbol{M}_i$ is

$$\boldsymbol{M}_i = \begin{bmatrix} \boldsymbol{0}_{4\times4} & \overline{\boldsymbol{m}}_i \\ \overline{\boldsymbol{J}}_i & \boldsymbol{0}_{4\times4} \end{bmatrix} \in \mathbb{R}^{8\times8} \tag{3}$$

where

$$\bar{\boldsymbol{J}}_i = \begin{bmatrix} 1 & \boldsymbol{0}_{1\times3} \\ \boldsymbol{0}_{3\times1} & \boldsymbol{J}_i \end{bmatrix} \in \mathbb{R}^{4\times4}, \overline{\boldsymbol{m}}_i = \begin{bmatrix} 1 & \boldsymbol{0}_{1\times3} \\ \boldsymbol{0}_{3\times1} & m_i\boldsymbol{I}_{3\times3} \end{bmatrix} \in \mathbb{R}^{4\times4}$$

Remark 1. As an extension of quaternion, the dual quaternion is one of the most commonly used methods for modeling the six-degrees-of-freedom coupled spacecraft. In contrast with other six-degree-of-freedom modeling methods, such as the Vectrix approach [33] and the Cayley description [34], the dual quaternion approach is more explicit in physical meaning and compact in its mathematical description. In particular, the introduction of dual numbers allows us to describe the six-degrees-of-freedom coupled dynamics with a unified equation, implying that we do not have to design separate controllers and Lyapunov functions for the rotational and translational parts of spacecraft.

Equation (1) and Equation (2) can be rewritten as

$$\begin{cases} \dot{\boldsymbol{x}}_i = \boldsymbol{v}_i \\ \dot{\boldsymbol{v}}_i = \boldsymbol{f}_i(\boldsymbol{x}_i, \boldsymbol{v}_i) + \boldsymbol{g}_i(\boldsymbol{x}_i)\, \boldsymbol{sat}\big[\boldsymbol{Q}(\boldsymbol{u}_i)\big] + \boldsymbol{d}_i \end{cases} \tag{4}$$

where $\boldsymbol{x}_i = \hat{\boldsymbol{q}}_i = \left[\hat{\boldsymbol{q}}_{ir}^{\mathrm{T}} \quad \hat{\boldsymbol{q}}_{id}^{\mathrm{T}}\right]^{\mathrm{T}}, \boldsymbol{v}_i = \dot{\hat{\boldsymbol{q}}}_i = \left[\dot{\hat{\boldsymbol{q}}}_{ir}^{\mathrm{T}} \quad \dot{\hat{\boldsymbol{q}}}_{id}^{\mathrm{T}}\right]^{\mathrm{T}}$, $\boldsymbol{f}_i(\boldsymbol{x}_i, \boldsymbol{v}_i) = \dot{\boldsymbol{\Gamma}}(\boldsymbol{x}_i)\, \boldsymbol{\Gamma}^{-1}(\boldsymbol{x}_i)\, \boldsymbol{v}_i - \boldsymbol{\Gamma}(\boldsymbol{x}_i)\, \boldsymbol{M}_i^{-1}\boldsymbol{Z}(\boldsymbol{x}_i, \boldsymbol{v}_i)$ $\boldsymbol{\Gamma}(\boldsymbol{x}_i)\, \boldsymbol{M}_i^{-1}\boldsymbol{G}$, $\boldsymbol{g}_i(\boldsymbol{x}_i) = \boldsymbol{\Gamma}(\boldsymbol{x}_i)\, \boldsymbol{M}_i^{-1}$, $\boldsymbol{u}_i = \left[\boldsymbol{f}_{ic}^{\mathrm{T}} \quad \boldsymbol{\tau}_{ic}^{\mathrm{T}}\right]^{\mathrm{T}}$, $\boldsymbol{d}_i = \boldsymbol{g}_i(\boldsymbol{x}_i)\left[\boldsymbol{f}_{ip}^{\mathrm{T}} \quad \boldsymbol{\tau}_{ip}^{\mathrm{T}}\right]^{\mathrm{T}}$, $\boldsymbol{Z}(\boldsymbol{x}_i, \boldsymbol{v}_i) =$ $\boldsymbol{\Gamma}\left[\boldsymbol{\Gamma}^{-1}(\boldsymbol{x}_i)\, \boldsymbol{v}_i\right] \boldsymbol{M}_i \boldsymbol{\Gamma}^{-1}(\boldsymbol{x}_i)\, \boldsymbol{v}_i - \boldsymbol{\Gamma}\left\{\left[\boldsymbol{M}_i \Gamma^{-1}(\boldsymbol{x}_i)\, \boldsymbol{v}_i\right]^*\right\}\left[\boldsymbol{\Gamma}^{-1}(\boldsymbol{x}_i)\, \boldsymbol{v}_i\right]^*$, $G = \left[\boldsymbol{f}_{ig}^{\mathrm{T}} \quad \boldsymbol{\tau}_{ig}^{\mathrm{T}}\right]^{\mathrm{T}}$, the transformation matrix $\boldsymbol{\Gamma}(\boldsymbol{x}_i)$ is defined in Equation (63). $\boldsymbol{g}_i(\boldsymbol{x}_i)$ is invertible because $\boldsymbol{\Gamma}(\boldsymbol{x}_i)$ and $\boldsymbol{M}_i$ are invertible.

The quantiser in Equation (4) is given as $\boldsymbol{Q}(\boldsymbol{u}_i) = [Q(u_{i1}), Q(u_{i2}), \ldots, Q(u_{i8})]^{\mathrm{T}}$. In our work, $Q(u)$ denotes the hysteretic quantiser, as shown in Equation (5). The subscript i and j are omitted for brevity.

https://doi.org/10.1017/aer.2023.23 Published online by Cambridge University Press

$$Q(u(t))=\begin{cases} u_p\text{sign}(u), & \dfrac{u_p}{1+\delta}<|u|\le u_p,\dot{u}<0,\text{ or} \\ & u_i<|u|\le\dfrac{u_p}{1-\delta},\dot{u}>0 \\ u_p(1+\delta)\text{sign}(u), & u_i<|u|\le\dfrac{u_p}{1-\delta},\dot{u}<0,\text{ or} \\ & \dfrac{u_i}{1-\delta}<|u|\le\dfrac{u_i(1+\delta)}{(1-\delta)},\dot{u}>0 \\ 0, & 0\le|u|<\dfrac{u_{\min}}{1+\delta},\dot{u}<0,\text{ or} \\ & \dfrac{u_{\min}}{1+\delta}\le|u|\le u_{\min},\dot{u}>0, \\ Q(u\,(t^-)) & \dot{u}=0 \end{cases} \tag{5}$$

where $u_p=\rho^{1-p}u_{\min}(p=1,2,\dots)$, $\delta=(1-\rho)/(1+\rho)$, $u_{\min}>0$, $0<\rho<1$, and $Q(u(t))\in\{0,\pm u_p,\pm u_p(1+\delta),p=1,2,\dots\}$. Besides, $u_{\min}>0$ denotes the range of the dead-zone for $Q(u(t))$, and $\rho>0$ represents a measure of quantisation density. We decompose the quantiser Equation (5) into $Q(u_{ij})=\chi_{qij}(u_{ij})\,u_{ij}+d_{qij},j=1,2,\cdots,8$, where

$$\chi_{qij}(u_{ij})=\begin{cases}\dfrac{Q(u_{ij})}{u_{ij}}, & Q(u_{ij})\neq 0,\\ 1, & Q(u_{ij})=0,\end{cases}$$

$$d_{qij}(u_{ij})=\begin{cases}0, & q(u_{ij})\neq 0,\\ -u_{ij}, & Q(u_{ij})=0.\end{cases}$$

It can be easily proven that the control coefficient χ_{qij} and the disturbance-like term d_{qij} satisfy $1-\delta\le\chi_{qij}\le 1+\delta$, $|d_{qij}|\le u_{\min}$. Thus, we can rewritten the quantiser as

$$\boldsymbol{Q}(\boldsymbol{u}_i)=\boldsymbol{\chi}_q(\boldsymbol{u}_i)\,\boldsymbol{u}_i+\boldsymbol{d}_q \tag{6}$$

where $\boldsymbol{\chi}_q(\boldsymbol{u}_i)=\text{diag}\left[\chi_{qi1}(u_{i1}),\chi_{qi2}(u_{i2}),\cdots,\chi_{qi8}(u_{i8})\right]^{\text{T}}$, $\boldsymbol{d}_q(\boldsymbol{u}_i)=\text{diag}\left[d_{qi1}(u_{i1}),d_{qi2}(u_{i2}),\cdots,d_{qi8}(u_{i8})\right]^{\text{T}}$.

Define $[\underline{M},\overline{M}]$ as the magnitude constraint of the actuator. The saturation nonlinearity in Equation (4) is given as

$$\boldsymbol{sat}(\boldsymbol{x})=\boldsymbol{\chi}_s(\boldsymbol{x})\,\boldsymbol{x}=[sat(x_1),sat(x_2),\cdots,sat(x_k)]^{\text{T}} \tag{7}$$

where $\boldsymbol{\chi}_s(\boldsymbol{x})=\text{diag}[\chi_{s1}(x_1),\chi_{s2}(x_2),\cdots,\chi_{sk}(x_k)]^{\text{T}}$ with

$$\chi_{sk}(x)=\begin{cases}\overline{M}/x, & \text{if } x\ge\overline{M}_u\\ 1, & \text{if } \underline{M}_u\le x\le\overline{M}_u\\ \underline{M}_u/x, & \text{if } x\le\underline{M}_u\end{cases}$$

such that $0<\chi_{sk}<1$. We can rewritten the term $\boldsymbol{sat}\left[\boldsymbol{Q}(\boldsymbol{u}_i)\right]$ in Equation (4) as

$$\boldsymbol{sat}\left[\boldsymbol{Q}(\boldsymbol{u}_i)\right]=\boldsymbol{\chi}(\boldsymbol{u}_i)\,\boldsymbol{u}_i+\boldsymbol{d}_{sq} \tag{8}$$

where $\boldsymbol{\chi}(\boldsymbol{u}_i)=\boldsymbol{\chi}_s(\boldsymbol{u}_i)\,\boldsymbol{\chi}_q(\boldsymbol{u}_i)$, $\boldsymbol{d}_{sq}=\boldsymbol{\chi}_s\boldsymbol{d}_q$.

2.3 Graph theory

We use an undirected graph $\boldsymbol{G}=\{\upsilon,\varsigma,\boldsymbol{A}\}$ to describe the communication topology of a formation with n spacecrafts, where the node set $\upsilon=\{\upsilon_1,\upsilon_2,\cdots,\upsilon_n\}$, the edge set $\varsigma\subseteq\upsilon\times\upsilon$, and the adjacency

https://doi.org/10.1017/aer.2023.23 Published online by Cambridge University Press

matrix $\boldsymbol{A} = [a_{ij}] \in \mathbb{R}^{n\times n}(i = 1, 2, \cdots, n; j = 1, 2, \cdots, n)$. If node υ_i can directly obtain the information of node υ_j, there is an edge in the graph from υ_j points to υ_i, denoted as $(\upsilon_i, \upsilon_j) \in \boldsymbol{\varsigma}$, and υ_j is the child node of υ_i. For an undirected graph, if an edge connects υ_i and υ_j, then the two are parent-child nodes, that is, if $(\upsilon_i, \upsilon_j) \in \boldsymbol{\varsigma}$, then $(\upsilon_j, \upsilon_i) \in \boldsymbol{\varsigma}$. In the adjacency matrix $\boldsymbol{A}$, $a_{ij} > 0$ if $(\upsilon_i, \upsilon_j) \in \boldsymbol{\varsigma}$; otherwise, $a_{ij} = 0$. Generally, it is assumed that $a_{ii} = 0$. The Laplace matrix $\boldsymbol{L}$ of graph $\boldsymbol{G}$ is defined as $\boldsymbol{L} = \text{diag}\left\{\sum_{j=1}^{n} a_{1j}, \cdots, \sum_{j=1}^{n} a_{nj}\right\} - \boldsymbol{A}$. For undirected graphs, the Laplace matrix $\boldsymbol{L}$ is symmetric.

Additionally, denote the virtual leader as spacecraft 0, of which states are given by $\boldsymbol{x}_0$ and $\boldsymbol{v}_0$. A leader-following graph $\overline{\boldsymbol{G}}$ contains the virtual leader and the original graph $\boldsymbol{G}$ of n follower spacecraft. $b_i = 1$ if the ith follower spacecraft can access the virtual leader spacecraft directly, and $b_i = 0$, otherwise. The graph $\overline{\boldsymbol{G}}$ is connected if there exists a path in $\overline{\boldsymbol{G}}$ from the leader node υ_0 to every node υ_i. If $\overline{\boldsymbol{G}}$ is connected, the matrix $\boldsymbol{L} + \boldsymbol{B}$ associated with $\overline{\boldsymbol{G}}$ is symmetric and positive definite [35], where $\boldsymbol{B} = \text{diag}(b_1, \cdots, b_2)$.

2.4 Problem statement

This paper committed to developing a distributed control scheme such that all follower spacecraft can track the virtual leader with the desired formation shape considering limited communication, i.e., $\lim_{t\to T} \left\|\boldsymbol{x}_i - \boldsymbol{\Delta}_{i,0} - \boldsymbol{x}_0\right\| \le o_1, \lim_{t\to T} \left\|\boldsymbol{v}_i - \dot{\boldsymbol{\Delta}}_{i,0} - \boldsymbol{v}_0\right\| \le o_2$, where $\boldsymbol{\Delta}_{i,0}$ is the ith follower spacecraft's expected deviation formation vector relative to the virtual leader, and o_1, o_2 are compact sets around zero.

Remark 2. We consider the desired position deviation formation vector $\boldsymbol{\Delta}_{i,0}$ to be an internal parameter of the ith follower spacecraft, which can be obtained without external communication.

In order to get the main results of this paper, the following assumptions are adopted.

Assumption 1. *The desired states $\boldsymbol{x}_0$ and its first two derivatives are uniformly bounded such that $\|\boldsymbol{x}_0\| \le B_1$, $\|\dot{\boldsymbol{x}}_0\| \le B_2$, $\|\ddot{\boldsymbol{x}}_0\| \le B_3$, where B_1, B_2, B_3 are positive constants.*

Assumption 2. *The disturbance $\boldsymbol{d}_i$ is bounded and satisfies $\|\boldsymbol{d}_i\| \le d_{max}$, where d_{max} is a positive constant.*

Assumption 3. [36] *For a constant χ_{min}, we consider the control input restricted in a region such that $\chi_{min} \le \chi_{sk} < 1$.*

Assumption 4. [37, 38] *For the practical SFF system described by Equation (4) with input saturation, $\boldsymbol{g}_i(\boldsymbol{x}_i)$ should be bounded and satisfies $\|\boldsymbol{g}_i(\boldsymbol{x}_i)\| \le g_{max}$.*

3.0 Distributed control scheme design

The procedure for designing the distributed control scheme is presented in this section. Firstly, a distributed event-triggered observer is designed with continuous communications, based on which we proposed an event-based distributed observer without continuous communications. Further, a distributed fixed-time controller is proposed for the follower spacecraft in the presence of the actuator saturation and the input quantisation problems. The block diagram of the distributed control algorithm is given in Fig. 2.

Remark 3. For the following reasons, we only add ETM in the observer, even though both the observer and the controller occupy communication resources. Firstly, the communication resources saved by ETM come at the cost of system performance; secondly, since the observer converges much faster than the controller, embedding the event-triggered mechanism in the observer has minimal impact on the system performance. If ETM is also embedded in the controller, it will save communication resources, but the system performance will be significantly reduced.

https://doi.org/10.1017/aer.2023.23 Published online by Cambridge University Press

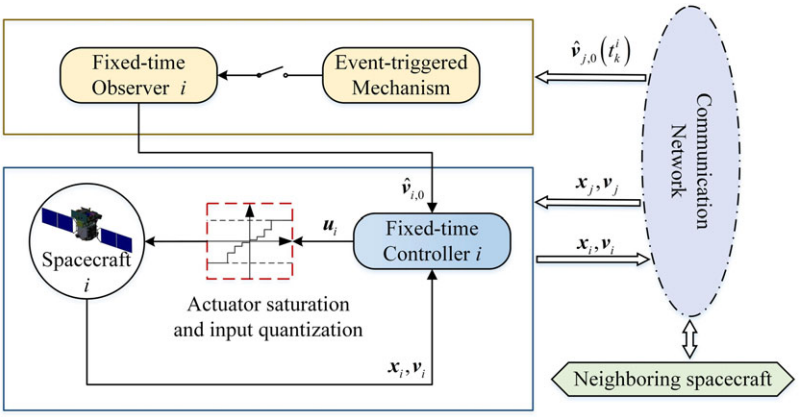

Figure 2. *Schematic of the distributed control algorithm.*

3.1 Event-triggered fixed-time observer design

This subsection develops the event-triggered fixed-time observer with continuous and without continuous communications to reconstruct the virtual leader spacecraft's information.

Define a auxiliary variable as $\boldsymbol{\zeta}_i = \sum_{j=1}^{n} a_{ij}\left(\hat{\boldsymbol{v}}_{i,0} - \hat{\boldsymbol{v}}_{j,0}\right) + b_i\left(\hat{\boldsymbol{v}}_{i,0} - \boldsymbol{v}_0\right)$ where $\hat{\boldsymbol{v}}_{i,0}$ denotes the estimation of $\boldsymbol{v}_0$ of the ith follower spacecraft, $\tilde{\boldsymbol{v}}_i = \hat{\boldsymbol{v}}_{i,0} - \boldsymbol{v}_0$ is the estimation error, $\tilde{\boldsymbol{v}} = \left[\tilde{\boldsymbol{v}}_1^{\mathrm{T}}, \tilde{\boldsymbol{v}}_2^{\mathrm{T}}, \ldots, \tilde{\boldsymbol{v}}_n^{\mathrm{T}}\right]^{\mathrm{T}}$, $\boldsymbol{\zeta} = \boldsymbol{H}\tilde{\boldsymbol{v}} = \left[\boldsymbol{\zeta}_1^{\mathrm{T}}, \boldsymbol{\zeta}_2^{\mathrm{T}}, \ldots, \boldsymbol{\zeta}_n^{\mathrm{T}}\right]^{\mathrm{T}}$.

3.1.1 Event-triggered fixed-time observer with continuous communications

The event-triggered fixed-time observer with continuous communications for the ith follower spacecraft is described as:

$$\begin{aligned}\dot{\hat{\boldsymbol{v}}}_{i,0} = \dot{\hat{\boldsymbol{v}}}_{i,0}(t_k) = &-o_1 \mathrm{sig}^{\frac{1}{\alpha}}\left[\boldsymbol{\zeta}_i(t_k)\right] - o_2 \mathrm{sig}^{\beta}\left[\boldsymbol{\zeta}_i(t_k)\right] \\ &-o_3 \mathrm{sig}^{\alpha}\left[\boldsymbol{\zeta}_i(t_k)\right] - o_4 \mathrm{obsat}\left[\boldsymbol{\zeta}_i(t_k)\right]\end{aligned} \tag{9}$$

$$t_{k+1} = \inf\left\{t > t_k : h_{ij} > 0, \forall j, j = 1, \cdots, 8\right\} \tag{10}$$

where

$$h_{ij}(t) = \left|E_{ij}(t)\right| - \iota\left|v_{uij}\right| - k_{o1}\sqrt{e^{1+k_{o2}\tanh\left(k_{o3}\left|\zeta_{ij}(t)\right|\right)}} \tag{11}$$

With $0 < \alpha < 1$, $\beta > 1$, $\iota \in (0,1)$, $o_1, o_2, o_3, o_4, k_{o1}, k_{o2}, k_{o3}$ are positive observer parameters, which will be chosen later. $\boldsymbol{E}_i(t) = \left[E_{i1}, \cdots, E_{ij}, \cdots\right]^{\mathrm{T}} = o_1 \mathrm{sig}^{\frac{1}{\alpha}}\left[\boldsymbol{\zeta}_i(t_k)\right] + o_2 \mathrm{sig}^{\beta}\left[\boldsymbol{\zeta}_i(t_k)\right] + o_3 \mathrm{sig}^{\alpha}\left[\boldsymbol{\zeta}_i(t_k)\right] + o_4 \mathrm{obsat}\left[\boldsymbol{\zeta}_i(t_k)\right] - o_1 \mathrm{sig}^{\frac{1}{\alpha}}\left[\boldsymbol{\zeta}_i(t)\right] - o_2 \mathrm{sig}^{\beta}\left[\boldsymbol{\zeta}_i(t)\right] - o_3 \mathrm{sig}^{\alpha}\left[\boldsymbol{\zeta}_i(t)\right] - o_4 \mathrm{obsat}\left[\boldsymbol{\zeta}_i(t)\right] = -\dot{\hat{\boldsymbol{v}}}_{i,0}(t_k) - \boldsymbol{v}_{ui}(t)$ where $\boldsymbol{v}_{ui}(t) = o_1 \mathrm{sig}^{\frac{1}{\alpha}}\left[\boldsymbol{\zeta}_i(t)\right] + o_2 \mathrm{sig}^{\beta}\left[\boldsymbol{\zeta}_i(t)\right] + o_3 \mathrm{sig}^{\alpha}\left[\boldsymbol{\zeta}_i(t)\right] + o_4 \mathrm{obsat}\left[\boldsymbol{\zeta}_i(t)\right]$. $\mathrm{obsat}(\boldsymbol{x}) = [\mathrm{obsat}(x_1), \cdots, \mathrm{obsat}(x_n)]^{\mathrm{T}}$ where $\mathrm{obsat}(x)$ is designed as:

$$\mathrm{obsat}(x) = \begin{cases} x/\delta_o, & |x| \le \delta_o \\ \mathrm{sign}(x), & |x| > \delta_o \end{cases} \tag{12}$$

Theorem 1. *Consider the system Equation (4) with the designed observer Equation (9) and the event-triggered updated rule Equation (10). Suppose* ***Assumption*** *1 holds. $\hat{\boldsymbol{v}}_i$ will estimate $\boldsymbol{v}_0$ in fixed time T_1 if the parameters satisfy $(1-\iota)o_4 > B_3 + k_{o1}\sqrt{e^{1+k_{o2}}}$. Meanwhile, there always exists a non-zero bound time for any two triggers, which means $t_{k+1} - t_k > \tau > 0$, and τ is a positive constant.*

https://doi.org/10.1017/aer.2023.23 Published online by Cambridge University Press

Proof. Consider the following Lyapunov function candidate:

$$V_\zeta = \frac{1}{2}\tilde{\boldsymbol{v}}^{\mathrm{T}}\boldsymbol{H}\tilde{\boldsymbol{v}} \tag{13}$$

where $\boldsymbol{H} = (\boldsymbol{L} + \boldsymbol{B}) \otimes \boldsymbol{I}_8$ describes the communication topology of the formation. The time derivative of Equation (13) along with Equation (9) is given by

$$\begin{aligned}
\dot{V}_\zeta &= \boldsymbol{\zeta}^{\mathrm{T}}\dot{\tilde{\boldsymbol{v}}}(t) = \boldsymbol{\zeta}^{\mathrm{T}}\left[\dot{\hat{\boldsymbol{v}}}(t) - \dot{\boldsymbol{v}}_{n0}\right] \\
&= -\boldsymbol{\zeta}^{\mathrm{T}}\left[\boldsymbol{E} + o_1\mathrm{sig}^{\frac{1}{\alpha}}(\boldsymbol{\zeta}) + o_2\mathrm{sig}^{\beta}(\boldsymbol{\zeta}) + o_3\mathrm{sig}^{\alpha}(\boldsymbol{\zeta}) + o_4\mathrm{obsat}\boldsymbol{\zeta}) + \dot{\boldsymbol{v}}_{n0}\right] \\
&\le |\boldsymbol{\zeta}|^{\mathrm{T}}|\boldsymbol{E}| - o_1\boldsymbol{\zeta}^{\mathrm{T}}\mathrm{sig}^{\frac{1}{\alpha}}(\boldsymbol{\zeta}) - o_2\boldsymbol{\zeta}^{\mathrm{T}}\mathrm{sig}^{\beta}(\boldsymbol{\zeta}) \\
&\quad -o_3\zeta^{\mathrm{T}}\mathrm{sig}^{\alpha}(\boldsymbol{\zeta}) - o_4\boldsymbol{\zeta}^{\mathrm{T}}\mathrm{obsat}(\boldsymbol{\zeta}) - \boldsymbol{\zeta}^{\mathrm{T}}\dot{\boldsymbol{v}}_{n0}
\end{aligned} \tag{14}$$

where $E = [E_1, E_2, \cdots, E_n]^{\mathrm{T}}$, $v_{n0} = [v_0, v_0, \cdots, v_0]^{\mathrm{T}} \in \mathbb{R}^{8n\times 1}$.

Considering the event-triggered update rule Equation (11) and **Assumption 1**, we can imply the following relationship from Equation (14):

$$\begin{aligned}
\dot{V}_\zeta &\le \boldsymbol{\zeta}|^{\mathrm{T}}|\boldsymbol{E}| - o_1\boldsymbol{\zeta}^{\mathrm{T}}\mathrm{sig}^{\frac{1}{\alpha}}(\boldsymbol{\zeta}) - o_2\boldsymbol{\zeta}^{\mathrm{T}}\mathrm{sig}^{\beta}(\boldsymbol{\zeta}) \\
&\quad -o_3\boldsymbol{\zeta}^{\mathrm{T}}\mathrm{sig}^{\alpha}(\boldsymbol{\zeta}) - o_4\boldsymbol{\zeta}^{\mathrm{T}}\mathrm{obsat}(\boldsymbol{\zeta}) + B_3\sum_{i=1}^{n}\sum_{j=1}^{8}\left|\zeta_{ij}\right| \\
&\le -o_1(1-\iota)\boldsymbol{\zeta}^{\mathrm{T}}\mathrm{sig}^{\frac{1}{\alpha}}(\boldsymbol{\zeta}) - o_2(1-\iota)\boldsymbol{\zeta}^{\mathrm{T}}\mathrm{sig}^{\beta}(\boldsymbol{\zeta}) - o_3(1-\iota)\boldsymbol{\zeta}^{\mathrm{T}}\mathrm{sig}^{\alpha}(\boldsymbol{\zeta}) \\
&\quad -o_4(1-\iota)\sum_{i=1}^{n}\sum_{j=1}^{8}\zeta_{ij}\mathrm{obsat}\left(\zeta_{ij}\right) + \left(B_3 + k_{o1}\sqrt{e^{1+k_{o2}}}\right)\sum_{i=1}^{n}\sum_{j=1}^{8}\left|\zeta_{ij}\right| \\
&\le -o_1(1-\iota)(8n)^{\frac{\alpha-1}{2\alpha}} \parallel \boldsymbol{\zeta} \parallel^{1+\frac{1}{\alpha}} - o_2(1-\iota)(8n)^{\frac{1-\beta}{2}} \parallel \boldsymbol{\zeta} \parallel^{1+\beta} - o_3(1-\iota) \parallel \boldsymbol{\zeta} \parallel^{1+\alpha} \\
&\quad -o_4(1-\iota)\sum_{i=1}^{n}\sum_{j=1}^{8}\zeta_{ij}\mathrm{obsat}\left(\zeta_{ij}\right) + \left(B_3 + k_{o1}\sqrt{e^{1+k_{o2}}}\right)\sum_{i=1}^{n}\sum_{j=1}^{8}\left|\zeta_{ij}\right|
\end{aligned} \tag{15}$$

where $-\boldsymbol{\zeta}^{T}\mathrm{sig}^{\alpha}(\boldsymbol{\zeta}) = -\sum_{i=1}^{n}\sum_{j=1}^{8}\left(\zeta_{ij}^2\right)^{\frac{1+\alpha}{2}} \le -\parallel \boldsymbol{\zeta} \parallel^{1+\alpha}$ and $-\boldsymbol{\zeta}^{T}\mathrm{sig}^{\beta}(\boldsymbol{\zeta}) = -\sum_{i=1}^{n}\sum_{j=1}^{8}\left(\zeta_{ij}^2\right)^{\frac{1+\beta}{2}} \le -(8n)^{\frac{1-\beta}{2}} \parallel \boldsymbol{\zeta} \parallel^{1+\beta}$ are derived by **Lemma 6** and **Lemma 7**.

Noting that $\sum_{i=1}^{n}\sum_{j=1}^{8}\zeta_{ij}\mathrm{obsat}\left(\zeta_{ij}\right) = \frac{1}{\delta_o}\sum\left(\bar{\zeta}_{ij}^2\right) + \sum\left|\bar{\zeta}_{ij}\right|$ where $\bar{\zeta}_{ij} = \left\{\zeta_{ij}\colon \left|\zeta_{ij}\right| \le \delta_o\right\}, \bar{\zeta}_{ij} = \left\{\zeta_{ij}\colon \left|\zeta_{ij}\right| > \delta_o\right\}$, $k \in [0, 8n]$.

For Equation (15), one has

$$\begin{aligned}
&-o_4(1-\iota)\sum_{i=1}^{n}\sum_{j=1}^{8}\zeta_{ij}\mathrm{obsat}\left(\zeta_{ij}\right) + \left(B_3 + k_{o1}\sqrt{e^{1+k_{02}}}\right)\sum_{i=1}^{n}\sum_{j=1}^{8}\left|\zeta_{ij}\right| \\
&\le -o_4(1-\iota)\left[\sum\left|\zeta_{ij}\right| + \frac{1}{\delta_o k}\left(\sum\left|\zeta_{ij}\right|\right)^2\right] \\
&\quad + \left(B_3 + k_{o1}\sqrt{e^{1+k_{02}}}\right)\sum\left|\zeta_{ij}\right| + \left(B_3 + k_{o1}\sqrt{e^{1+k_{o2}}}\right)\sum\left|\zeta_{ij}\right| \\
&\le -o_4(1-\iota)\frac{1}{\delta_o k}\left(\sum\left|\zeta_{ij}\right|\right)^2 + \left(B_3 + k_{o1}\sqrt{e^{1+k_{o2}}}\right)\sum\left|\zeta_{ij}\right|
\end{aligned}$$

https://doi.org/10.1017/aer.2023.23 Published online by Cambridge University Press

$$= -o_4(1-\iota)\sum|\zeta_{ij}| + \left(B_3 + k_{o1}\sqrt{e^{1+k_{02}}}\right)\sum|\zeta_{ij}|$$
$$-o_4(1-\iota)\frac{1}{\delta_o k}\left(\sum|\zeta_{ij}|\right)^2 + o_4(1-\iota)\sum|\zeta_{ij}|$$
$$\leq \frac{o_4(1-\iota)\delta_o k}{4} \tag{16}$$

when $k \neq 0$, where the inequalities $k\sum\left(\bar{\zeta}_{ij}^2\right) \geqslant \left(\sum|\bar{\zeta}_{ij}|\right)^2$ which are derived by **Lemma 6** has been used. It should be noticed that $-o_4(1-\iota)\sum_{i=1}^{n}\sum_{j=1}^{8}\zeta_{ij}\mathrm{obsat}(\zeta_{ij}) + \left(B_3 + k_{o1}\sqrt{e^{1+k_{02}}}\right)\sum_{i=1}^{n}\sum_{j=1}^{8}|\zeta_{ij}| \leq 0$ when $k = 0$. It seems that the discussion of whether $k = 0$ in Equation (16) is redundant from the results, but the application of **Lemma 6** introduces a singular term $\frac{1}{k}$. Therefore, the discussion above is necessary. We can rewrite Equation (15) as

$$\dot{V}_\zeta \leq -o_1(1-\iota)(8n)^{\frac{\alpha-1}{2\alpha}} \parallel \boldsymbol{\zeta} \parallel^{1+\frac{1}{\alpha}} - o_2(1-\iota)(8n)^{\frac{1-\beta}{2}} \parallel \boldsymbol{\zeta} \parallel^{1+\beta}$$
$$-o_3(1-\iota) \parallel \boldsymbol{\zeta} \parallel^{1+\alpha} + \frac{o_4(1-\iota)\delta_o k}{4} \tag{17}$$

Noting that $V_\zeta = \frac{1}{2}\tilde{\boldsymbol{v}}^{\mathrm{T}}H\tilde{\boldsymbol{v}} = \frac{1}{2}\boldsymbol{\zeta}^{\mathrm{T}}H^{-1}\boldsymbol{\zeta} \leq \frac{1}{2\lambda_{\min}(H)} \parallel \boldsymbol{\zeta} \parallel^2$, Equation (17) becomes

$$\dot{V}_\zeta \leq -o_2(1-\iota)(8n)^{\frac{1-\beta}{2}}[2\lambda_{\min}(\boldsymbol{H})]^{\frac{1+\beta}{2}}V_\zeta^{\frac{1+\beta}{2}}$$
$$-o_3(1-\iota)[2\lambda_{\min}(\boldsymbol{H})]^{\frac{1+\alpha}{2}}V_\zeta^{\frac{1+\alpha}{2}} + \frac{o_4(1-\iota)\boldsymbol{\delta}_o k}{4} \tag{18}$$

which implies that V_ζ converges to a small neighbourhood of zero in fixed time $T_1 \leq 1/\left[\kappa_1\left(1-\frac{1+\alpha}{2}\right)\right] + 1/\left[\kappa_2\left(\frac{1+\beta}{2}-1\right)\right]$ where $\kappa_1 = o_3(1-\iota)[2\lambda_{\min}(\boldsymbol{H})]^{\frac{1+\alpha}{2}}$, $\kappa_2 = o_2(1-\iota)(8n)^{\frac{1-\beta}{2}}[2\lambda_{\min}(\boldsymbol{H})]^{\frac{1+\beta}{2}}$. Thus, we conclude that the estimation error $\widetilde{\boldsymbol{v}_i} = \hat{\boldsymbol{v}}_i - \boldsymbol{v}_0$ converges to a small neighbourhood of zero in fixed time.

For $\boldsymbol{E}_i(t) = o_1\mathrm{sig}^{\frac{1}{\alpha}}\left[\boldsymbol{\zeta}_i(t_k)\right] + o_2\mathrm{sig}^{\beta}\left[\boldsymbol{\zeta}_i(t_k)\right] + o_3\mathrm{sig}^{\alpha}\left[\boldsymbol{\zeta}_i(t_k)\right] + o_4\mathrm{sign}\left[\boldsymbol{\zeta}_i(t_k)\right] - o_1\mathrm{sig}^{\frac{1}{\alpha}}\left[\boldsymbol{\zeta}_i(t)\right] - o_2\mathrm{sig}^{\beta}\left[\boldsymbol{\zeta}_i(t)\right] - o_3\mathrm{sig}^{\alpha}\left[\boldsymbol{\zeta}_i(t)\right] - o_4\mathrm{sign}\left[\boldsymbol{\zeta}_i(t)\right]$, we have

$$\left|\dot{E}_{ij}(t)\right| = \left|\left[o_1\mathrm{sig}^{\frac{1}{\alpha}}(\zeta_{ij}) + o_2\mathrm{sig}^{\beta}(\zeta_{ij}) + o_3\mathrm{sig}^{\alpha}(\zeta_{ij}) + o_4\mathrm{obsat}(\zeta_{ij})\right]'\right|$$
$$\leq \left|o_1\frac{1}{\alpha}\mathrm{sig}^{\frac{1-\alpha}{\alpha}}(\zeta_{ij}) + o_2\beta\mathrm{sig}^{\beta-1}(\zeta_{ij}) + o_3\alpha\mathrm{sig}^{\alpha-1}(\zeta_{ij}) + \frac{1}{\delta_o}\right|\left|\dot{\zeta}_{ij}\right| \tag{19}$$

From Equation (18) we know that ζ_{ij} is bounded, then we define the upper bound of $\left|o_1\frac{1}{\alpha}\mathrm{sig}^{\frac{1-\alpha}{\alpha}}(\zeta_{ij}) + o_2\beta\mathrm{sig}^{\beta-1}(\zeta_{ij}) + o_3\alpha\mathrm{sig}^{\alpha-1}(\zeta_{ij}) + \frac{1}{\delta_o}\right|$ as η_1. Equation (19) can be transformed into:

$$\left|\dot{E}_{ij}(t)\right| \leq \eta_1\left|\dot{\zeta}_{ij}\right| \leq \eta_1 h_{\max}\left[\dot{\hat{v}}_{ij}(t) - \dot{v}_{0ij}(t_k)\right]$$
$$\leq \eta_1 h_{\max}\left|\eta_{2ij}(t_k) + B_3\right| \tag{20}$$

where h_{max} is the largest element in matrix $\boldsymbol{H}$, $\eta_{2ij}(t_k) = o_1\mathrm{sig}^{\frac{1}{\alpha}}\left[\zeta_{ij}(t_k)\right] + o_2\mathrm{sig}^{\beta}\left[\zeta_{ij}(t_k)\right] + o_3\mathrm{sig}^{\alpha}\left[\zeta_{ij}(t_k)\right] + o_4\mathrm{sign}\left[\zeta_{ij}(t_k)\right]$. Since $\dot{E}_{ij}(t_k) = 0$, it follows when $t > t_k$:

$$\left|E_{ij}(t)\right| \leq \int_{t_k}^{t}\eta_1 h_{\max}\left|\eta_{2ij}(t_k) + B_3\right|\mathrm{d}s \tag{21}$$

According to the triggering condition Equation (11), one has that the next event of state j of agent i will not be triggered before $h_{ij}(t) = 0$ or equivalently $\left|E_{ij}(t)\right| = \iota o_2\mathrm{sig}^{\beta}\left(\left|\zeta_{ij}(t)\right|\right) + \iota o_3\mathrm{sig}^{\alpha}\left(\left|\zeta_{ij}(t)\right|\right) + k_{o1}\sqrt{e^{1+k_{o2}\tanh\left(\left|\zeta_{ij}(t)\right|\right)}}$. From Equation (21), one has:

https://doi.org/10.1017/aer.2023.23 Published online by Cambridge University Press

$$\begin{aligned}\left|E_{ij}(t_{k+1})\right| &= \iota o_2 \mathrm{sig}^{\beta}\left(\left|\zeta_{ij}(t_{k+1})\right|\right) + \iota o_3 \mathrm{sig}^{\alpha}\left(\left|\zeta_{ij}(t_{k+1})\right|\right) \\ &\quad + k_{o1}\sqrt{e^{1+k_{o2}\tanh\left(\left(\xi_{ij}(t_{k+1})\right|\right)}} \\ &\leq \int_{t_k}^{t_{k+1}} \eta_1 h_{\max}\left|\eta_{2ij}(t_k) + B_3\right| \mathrm{d}s \\ &\leq \int_{t_k}^{t_{k+1}} \eta_1 h_{\max}\left|\eta_{2ij\max} + B_3\right| \mathrm{d}s \end{aligned} \tag{22}$$

where $\eta_{2ij\max}$ is the upper bound of $\eta_{2ij}(t_k)$. Equation (22) yields that $t_{k+1} - t_k \geqslant k_{o1}\sqrt{e}/\left(\eta_1 h_{\max}\left|\eta_{2ij\max} + B_3\right|\right)$, which is shown that Zeno-free is guaranteed. □

3.1.2 Event-triggered fixed-time observer without continuous communications

This subsection proposes the event-triggered fixed-time observer without continuous communications based on subsection 3.1.1.

For the ith follower spacecraft, $\dot{\hat{v}}_i$ is the same as Equation (9). The triggering condition is described as:

$$t_{k+1} = \inf\left\{t > t_k : g_{ij} > 0, \forall j, j = 1, \cdots, 8\right\} \tag{23}$$

where

$$\begin{aligned} g_{ij}(t) &= \int_{t_k}^{t} \eta_1 h_{\max}\left|\eta_{2ij}(t_k) + B_3\right| \mathrm{d}s \\ &\quad - \frac{\iota}{1+\iota}\left|-\dot{\hat{v}}_{ij}(t_k) + \frac{k_{o1}}{\iota}\sqrt{e^{1+k_{o2}\tanh\left(k_{o3}\left|\xi_{ij}(t_k)\right|\right)}}\right| \end{aligned} \tag{24}$$

Theorem 2. *Consider the system Equation (4) with the designed observer Equation (9) and the event-triggered updated rule Equation (24). Suppose Assumption 1 holds. $\hat{\boldsymbol{v}}_i$ will estimate $\boldsymbol{v}_0$ in fixed time T_1 if the parameters satisfy $(1-\iota)o_4 > B_3 + k_{o1}\sqrt{e^{1+k_{o2}}}$.. Meanwhile, there always exists a non-zero bound time for any two triggers, which means $t_{k+1} - t_k > \tau > 0$, and τ is a positive constant.*

Proof. According to Equation (21), we can obtain $\left|E_{ij}(t)\right| \leq \int_{t_k}^{t} \eta_1 h_{\max}\left|\eta_{2ij}(t_k) + B_3\right| ds$, $t \in [t_k, t_{k+1})$. Further, the triggering function Equation (24) enforces

$$\left|E_{ij}(t)\right| \leq \frac{\iota}{1+\iota}\left|-\dot{\hat{v}}_{ij}(t_k) + \frac{k_{o1}}{\iota}\sqrt{e^{1+k_{o2}\tanh\left(\left|\zeta_{ij}(t_k)\right|\right)}}\right| \tag{25}$$

Noting that $E_{ij} = -\dot{\hat{v}}_{ij}(t_k) - v_{uij}$, Equation (25) can be transformed into

$$\left|E_{ij}(t)\right| + \iota\left|\dot{\hat{v}}_{ij}(t_k) + v_{ui}\right| \leq \iota\left|\dot{\hat{v}}_{ij}(t_k)\right| + k_{o1}\sqrt{e^{1+k_{o2}\tanh\left(\left|\zeta_{ij}(t_k)\right|\right)}} \tag{26}$$

which is is a sufficient condition for

$$\left|E_{ij}(t)\right| \leq \iota\left|v_{uij}\right| + k_{o1}\sqrt{e^{1+k_{o2}\tanh\left(\left|\zeta_{ij}(t)\right|\right)}} \tag{27}$$

Equation (27) is the same as the event-triggered updated rule Equation (11). Hence, similar to the proof of **Theorem 1**, the estimation error $\tilde{\hat{\boldsymbol{v}}}_i = \hat{\boldsymbol{v}}_i - \boldsymbol{v}_0$ converges to a small neighbourhood of zero in fixed time $T_1 \leq 1/\left[\kappa_1\left(1 - \frac{1+\alpha}{2}\right)\right] + 1/\left[\kappa_2\left(\frac{1+\beta}{2} - 1\right)\right]$, and Zeno-free is guaranteed. □

Remark 4. Compared with the distributed fixed-time observer in [12], an additional term $\mathrm{sig}^{\frac{1}{\alpha}}\left[\boldsymbol{\zeta}_i(t_k)\right]$ is adopted in Equation (9) to handle certain nonlinear term generated by the fixed-time controller. As

https://doi.org/10.1017/aer.2023.23 Published online by Cambridge University Press

shown in Equation (43), we guarantee the fixed time stability of the entire closed-loop system without recourse to the separation principle. Besides, the observer introduces an ETM without continuous communications, reducing energy consumption significantly.

Remark 5. The sign function results in adverse chattering. Differing from the work of [12], the saturation function is used in place of the sign function for the alleviation of chattering. The constant term $\frac{o_4(1-\iota)\delta k}{4}$ is thus introduced in Equation (18), implying that V_ζ converges to a region. Nonetheless, the region can be as small as desired by selecting parameter δ. The region is correspondingly scaled down to a smaller neighbourhood of the origin and the error caused by the approximation is negligible.

Remark 6. The ETM without continuous communications in Equation (24) is inspired by [17], where the event-triggered mechanism is used in a consensus control scheme. Differently, Equation (24) embeds a bounded nonlinear term $\frac{k_{o1}}{\iota}\sqrt{e^{1+k_{o2}\tanh\left(k_{o3}\left|\xi_{ij}(t_k)\right|\right)}}$, which realises a more reasonable trigger threshold with characteristics of the exponential function and the hyperbolic tangent function in the transient and steady state.

Remark 7. In view of Equation (24), the key rules in selecting the parameters are: The trigger interval can be increased by increasing the parameter k_{o1}. Subsequently, tuning the parameter k_{o2} can adjust the exponential convergence rate of the triggering condition during the adjustment period. Meanwhile, the selection of k_{o3} should ensure that $k_{o3}\left|\xi_{ij}(t_k)\right|$ can cover the unsaturated area of the hyperbolic tangent function.

3.2 Fixed-time controller design

In this subsection, a fixed-time distributed control scheme is designed for each follower spacecraft, handling the actuator saturation and the input quantisation problems ingeniously without embedding auxiliary systems. Define a auxiliary vector for *i*th follower spacecraft as

$$\begin{aligned}\boldsymbol{\sigma}_i &= \sum_{j=1}^{n} a_{ij}\left[(\boldsymbol{x}_i - \boldsymbol{\Delta}_{i,0}) - (\boldsymbol{x}_j - \boldsymbol{\Delta}_{j,str})\right] + b_i\left(\boldsymbol{x}_i - \boldsymbol{\Delta}_{i,0} - \boldsymbol{x}_0\right)\\ &= \sum_{j=1}^{n} l_{ij}\boldsymbol{e}_{xj} + b_i\boldsymbol{e}_{xi}\end{aligned} \tag{28}$$

where $\boldsymbol{e}_{xi} = \boldsymbol{x}_i - \boldsymbol{\Delta}_{i,0} - \boldsymbol{x}_0$. Denote $\boldsymbol{\sigma} = \left[\boldsymbol{\sigma}_1^{\mathrm{T}}, \boldsymbol{\sigma}_2^{\mathrm{T}}, \ldots, \boldsymbol{\sigma}_n^{\mathrm{T}}\right]^{\mathrm{T}}$, $\boldsymbol{e}_x = \left[\boldsymbol{e}_{x1}^{\mathrm{T}}, \boldsymbol{e}_{x2}^{\mathrm{T}}, \ \ldots, \boldsymbol{e}_{xn}^{\mathrm{T}}\right]^{\mathrm{T}}$, then we have $\boldsymbol{\sigma} = \boldsymbol{H}\boldsymbol{e}_x$. Based on the backstepping technique, the controller is designed as follows:

Step 1. Design of a virtual control scheme for $\boldsymbol{\gamma}_i = \boldsymbol{v}_i - \hat{\boldsymbol{v}}_{i,0} - \dot{\boldsymbol{\Delta}}_{i,0} + k_1\mathrm{sig}^{\beta}(\boldsymbol{\sigma}_i)$, where k_1 is a positive parameter.

Consider $\boldsymbol{\gamma}_i$ as a virtual control input for the system $\dot{\boldsymbol{\sigma}} = \boldsymbol{H}\dot{\boldsymbol{e}}_x = \boldsymbol{H}\boldsymbol{e}_v = \boldsymbol{H}\left(\boldsymbol{v}_i - \hat{\boldsymbol{v}}_{i,0} - \dot{\boldsymbol{\Delta}}_{i,0} + \tilde{\boldsymbol{v}}_i\right)$, A virtual control scheme for $\boldsymbol{\gamma}_i$ is designed as $\boldsymbol{\gamma}_{di} = -k_2\mathrm{sig}^{\alpha}(\boldsymbol{\sigma}_i)$, where k_1 is a positive parameter, $\boldsymbol{e}_v = \left[\boldsymbol{e}_{v1}^{\mathrm{T}}, \boldsymbol{e}_{v2}^{\mathrm{T}}, \ldots, \boldsymbol{e}_{vn}^{\mathrm{T}}\right]^{\mathrm{T}}$, $\boldsymbol{e}_{vi} = \boldsymbol{v}_i - \dot{\boldsymbol{\Delta}}_{i,0} - \boldsymbol{v}_0$.

Consider the following Lyapunov function candidate

$$V_1 = \frac{1}{2}\boldsymbol{\sigma}^{\mathrm{T}}\boldsymbol{H}^{-1}\boldsymbol{\sigma} \tag{29}$$

and the time derivative of V_1 is given by

$$\begin{aligned}\dot{V}_1 &= \boldsymbol{\sigma}^{\mathrm{T}}\boldsymbol{e}_v = \boldsymbol{\sigma}^{\mathrm{T}}\left(\boldsymbol{v} - \hat{\boldsymbol{v}} - \dot{\boldsymbol{\Delta}}_{str} + \tilde{\boldsymbol{v}}\right) = \boldsymbol{\sigma}^{T}(\boldsymbol{\gamma} + \tilde{\boldsymbol{v}})\\ &= \boldsymbol{\sigma}^{\mathrm{T}}\left(\boldsymbol{\gamma} - \boldsymbol{\gamma}_d\right) + \boldsymbol{\sigma}^{\mathrm{T}}\tilde{\boldsymbol{v}} - k_1\boldsymbol{\sigma}^{\mathrm{T}}\mathrm{sig}^{\beta}(\boldsymbol{\sigma}) - k_2\boldsymbol{\sigma}^{\mathrm{T}}\mathrm{sig}^{\alpha}(\boldsymbol{\sigma})\end{aligned} \tag{30}$$

where $\boldsymbol{\gamma} = \left[\boldsymbol{\gamma}_1{}^{\mathrm{T}}, \boldsymbol{\gamma}_2{}^{\mathrm{T}}, \ldots, \boldsymbol{\gamma}_n{}^{\mathrm{T}}\right]^{\mathrm{T}}$, $\boldsymbol{\gamma}_d = \left[\boldsymbol{\gamma}_{d1}{}^{\mathrm{T}}, \boldsymbol{\gamma}_{d2}{}^{\mathrm{T}}, \ldots, \boldsymbol{\gamma}_{dn}{}^{\mathrm{T}}\right]^{\mathrm{T}}$.

https://doi.org/10.1017/aer.2023.23 Published online by Cambridge University Press

According to **Lemma 2** and **Lemma 5**, we can imply the following unequal relationship:

$$\begin{aligned}\boldsymbol{\sigma}^{\mathrm{T}}(\boldsymbol{\gamma}-\boldsymbol{\gamma}_d) &\le \sum_{i=1}^{n}\sum_{j=1}^{8}\left|\sigma_{ij}\right|\left|\gamma_{ij}-\gamma_{dij}\right| \le \sum_{i=1}^{n}\sum_{j=1}^{8}2^{1-\alpha}\left|\sigma_{ij}\parallel\kappa_{ij}\right|^{\alpha}\\ &\le \frac{2^{1-\alpha}}{1+\alpha}\boldsymbol{\sigma}^{\mathrm{T}}\mathrm{sig}^{\alpha}(\boldsymbol{\sigma})+\frac{2^{1-\alpha}\alpha}{1+\alpha}\boldsymbol{\kappa}^{\mathrm{T}}\mathrm{sig}^{\alpha}(\boldsymbol{\kappa})\end{aligned} \tag{31}$$

$$\boldsymbol{\sigma}^{\mathrm{T}}\tilde{\boldsymbol{\nu}} \le \sum_{i=1}^{n}\sum_{j=1}^{8}\left|\sigma_{ij}\right|\left(\left|\tilde{\nu}_{ij}\right|^{\frac{1}{\alpha}}\right)^{\alpha} \le \frac{1}{1+\alpha}\boldsymbol{\sigma}^{\mathrm{T}}\mathrm{sig}^{\alpha}(\boldsymbol{\sigma})+\frac{\alpha}{1+\alpha}\tilde{\boldsymbol{\nu}}^{\mathrm{T}}\mathrm{sig}^{\frac{1}{\alpha}}(\tilde{\boldsymbol{\nu}}) \tag{32}$$

where $\kappa_{ij}=\mathrm{sig}^{\frac{1}{\alpha}}(\gamma_{ij})-\mathrm{sig}^{\frac{1}{\alpha}}(\gamma_{dij})$.

Substitution of Equation (31) and Equation (32) into Equation (30) yields that

$$\begin{aligned}\dot{V}_1 &\le -k_1\boldsymbol{\sigma}^{\mathrm{T}}\mathrm{sig}^{\beta}(\boldsymbol{\sigma})-\left(k_2-\frac{1+2^{1-\alpha}}{1+\alpha}\right)\boldsymbol{\sigma}^{\mathrm{T}}\mathrm{sig}^{\alpha}(\boldsymbol{\sigma})\\ &\quad+\frac{2^{1-\alpha}\alpha}{1+\alpha}\boldsymbol{\kappa}^{\mathrm{T}}\mathrm{sig}^{\alpha}(\boldsymbol{\kappa})+\frac{\alpha}{1+\alpha}\tilde{\boldsymbol{\nu}}^{\mathrm{T}}\mathrm{sig}^{\frac{1}{\alpha}}(\tilde{\boldsymbol{\nu}})\\ &\le -k_1\parallel\boldsymbol{\sigma}\parallel^{1+\beta}-\left(k_2-\frac{1+2^{1-\alpha}}{1+\alpha}\right)\parallel\boldsymbol{\sigma}\parallel^{1+\alpha}\\ &\quad+\frac{2^{1-\alpha}\alpha}{1+\alpha}\parallel\boldsymbol{\kappa}\parallel^{1+\alpha}+\frac{\alpha}{1+\alpha}\tilde{\boldsymbol{\nu}}\parallel^{1+\frac{1}{\alpha}}\end{aligned} \tag{33}$$

Step 2. Design of the control scheme for $\boldsymbol{u}_i$.

The distributed fixed-time control scheme is described as:

$$\begin{aligned}\boldsymbol{u}_i &= \boldsymbol{g}^{-1}(\boldsymbol{x}_i)\left[-\frac{\|\boldsymbol{F}_i\|^2\mathrm{sig}^{2-\alpha}(\boldsymbol{\kappa}_i)}{2\iota_f}-k_3\mathrm{sig}^{2\alpha-1}(\boldsymbol{\kappa}_i)\right]\\ &\quad+\boldsymbol{g}^{-1}(\boldsymbol{x}_i)\left[-k_4\mathrm{sig}^{\beta-1+\alpha}(\boldsymbol{\kappa}_i)-k_5\mathrm{sig}^{2-\alpha}(\boldsymbol{\kappa}_i)\right]\end{aligned} \tag{34}$$

where $\boldsymbol{F}_i=\boldsymbol{f}_i(\boldsymbol{x}_i,\boldsymbol{v}_i)-\dot{\hat{\boldsymbol{v}}}_{i,0}-\ddot{\boldsymbol{\Delta}}_{i,0}+k_1\beta\mathrm{sig}^{\beta-1}(\boldsymbol{\sigma}_i)\,\dot{\boldsymbol{\sigma}}_i$, k_3, k_4, k_5 and ι_f are positive parameters.

Theorem 3. *Suppose **Assumption** 2, 3 hold. With the implementation of the fixed-time observer Equation (9) and the control scheme Equation (34). The control parameters satisfy* $2k_5\chi_{min}(1-\delta)>\iota_d$, $k_1>\frac{c_1k_1\beta}{1+\beta}$, $k_2>\frac{1+2^{1-\alpha}}{1+\alpha}+\frac{c_3\alpha}{1+\alpha}$, $k_4\chi_{min}(1-\delta)(8n)^{\frac{1+\beta}{2}}>\frac{c_1k_1}{1+\beta}$, $k_3\chi_{min}(1-\delta)>c_1c_2+\frac{c_1+c_3}{1+\alpha}+\frac{2^{1-\alpha}\alpha}{1+\alpha}$, $o_1(1-\iota)(8n)^{\frac{\alpha-1}{2\alpha}}>\frac{(c_1+1)\alpha}{(1+\alpha)\lambda_{\min}(H)^{1+\frac{1}{\alpha}}}$. *Then the tracking errors $\boldsymbol{e}_{xi}$, $\boldsymbol{e}_{vi}$ for each follower spacecraft can converge to a region in fixed time T_2.*

Proof. Consider the following Lyapunov function candidate [30]:

$$V_2=\sum_{i=1}^{n}\sum_{j=1}^{8}\int_{\gamma_{dij}}^{\gamma_{ij}}\mathrm{sig}^{2-\alpha}\left(\mathrm{sig}^{\frac{1}{\alpha}}(s)-\mathrm{sig}^{\frac{1}{\alpha}}(\gamma_{dij})\right)\mathrm{d}s \tag{35}$$

then the time derivative of V_2 is given by

$$\dot{V}_2=\dot{\gamma}^{T}\mathrm{sig}^{2-\alpha}(\boldsymbol{\kappa})+\sum_{i=1}^{n}\sum_{j=1}^{8}\int_{\gamma_{dij}}^{\gamma_{ij}}\frac{\mathrm{d}}{\mathrm{d}t}\mathrm{sig}^{2-\alpha}\left(\mathrm{sig}^{\frac{1}{\alpha}}(s)-\mathrm{sig}^{\frac{1}{\alpha}}(\gamma_{dij})\right)\mathrm{d}s \tag{36}$$

https://doi.org/10.1017/aer.2023.23 Published online by Cambridge University Press

For the second term in the Equation (36), we could rewrite it as

$$\sum_{i=1}^{n}\sum_{j=1}^{8}\int_{\gamma_{dij}}^{\gamma_{ij}}\frac{\mathrm{d}}{\mathrm{d}t}\mathrm{sig}^{2-\alpha}\left(\mathrm{sig}^{\frac{1}{\alpha}}(s)-\mathrm{sig}^{\frac{1}{\alpha}}\left(\gamma_{dij}\right)\right)\mathrm{d}s=\sum_{i=1}^{n}\sum_{j=1}^{8}(2-\alpha)\,k_2^{\frac{1}{\alpha}}\dot{\sigma}_{ij}\Upsilon_{ij} \tag{37}$$

where

$$\Upsilon_{ij}=\int_{\gamma_{ij}}^{\gamma_{ij}}\mathrm{sig}^{1-\alpha}\left(\mathrm{sig}^{\frac{1}{\alpha}}(s)-\mathrm{sig}^{\frac{1}{\alpha}}\left(\gamma_{dij}\right)\right)\mathrm{d}s\le 2^{1-\alpha}\left|\kappa_{ij}\right| \tag{38}$$

which is obtained by **Lemma 2** and **Lemma 5**.

Substituting Equation (37) and Equation (38) into Equation (36), it can yield

$$\begin{aligned}\dot{V}_2&\le\dot{\boldsymbol{\gamma}}^{\mathrm{T}}\mathrm{sig}^{2-\alpha}(\boldsymbol{\kappa})+(2-\alpha)k_2^{\frac{1}{\alpha}}2^{1-\alpha}\dot{\boldsymbol{\sigma}}^{\mathrm{T}}|\kappa|\\&\le\dot{\boldsymbol{\gamma}}^{\mathrm{T}}\mathrm{sig}^{2-\alpha}(\kappa)\\&\quad+(2-\alpha)k_2^{\frac{1}{\alpha}}\lambda_{\max}(\boldsymbol{H})\parallel\boldsymbol{\kappa}\parallel\left\|\boldsymbol{\gamma}-\boldsymbol{\gamma}_d+\tilde{\boldsymbol{\nu}}-k_1\mathrm{sig}^{\beta}(\boldsymbol{\sigma})-k_2\mathrm{sig}^{\alpha}(\boldsymbol{\sigma})\right\|\end{aligned} \tag{39}$$

Noting that $\left\|\boldsymbol{\gamma}-\boldsymbol{\gamma}_d\right\|\le\sum_{i=1}^{n}\sum_{j=1}^{8}2^{1-\alpha}\left|\boldsymbol{\kappa}_{ij}\right|^{\alpha}\le 2^{1-\alpha}(8n)^{\frac{1-\alpha}{2}}\parallel\boldsymbol{\kappa}\parallel^{\alpha}$, $\left\|k_1\mathrm{sig}^{\beta}(\boldsymbol{\sigma})\right\|\le k_1\parallel\boldsymbol{\sigma}\parallel^{\beta}$, $\parallel k_2\mathrm{sig}^{\alpha}(\boldsymbol{\sigma})\parallel\le k_2(8n)^{\frac{1-\alpha}{2}}\parallel\boldsymbol{\sigma}\parallel^{\alpha}$ where **Lemma 2**, **Lemma 5** and **Lemma 6** are used, we have

$$\begin{aligned}\dot{V}_2&\le\dot{\boldsymbol{\gamma}}^{\mathrm{T}}\mathrm{sig}^{2-\alpha}(\boldsymbol{\kappa})+c_1c_2\parallel\boldsymbol{\kappa}\parallel^{1+\alpha}+c_1\parallel\boldsymbol{\kappa}\parallel\parallel\tilde{\boldsymbol{\nu}}\parallel+c_1k_1\parallel\boldsymbol{\kappa}\parallel\parallel\boldsymbol{\sigma}\parallel^{\beta}+c_3\parallel\boldsymbol{\kappa}\parallel\parallel\boldsymbol{\sigma}\parallel^{\alpha}\\&\le\dot{\boldsymbol{\gamma}}^{\mathrm{T}}\mathrm{sig}^{2-\alpha}(\boldsymbol{\kappa})+c_1c_2\parallel\boldsymbol{\kappa}\parallel^{1+\alpha}+c_1\left(\frac{1}{1+\alpha}\parallel\boldsymbol{\kappa}\parallel^{1+\alpha}+\frac{\alpha}{1+\alpha}\parallel\tilde{\boldsymbol{\nu}}\parallel^{1+\frac{1}{\alpha}}\right)\\&\quad+c_1k_1\left(\frac{1}{1+\beta}\parallel\boldsymbol{\kappa}\parallel^{1+\beta}+\frac{\beta}{1+\beta}\parallel\boldsymbol{\sigma}\parallel^{1+\beta}\right)+c_3\left(\frac{1}{1+\alpha}\boldsymbol{\kappa}\parallel^{1+\alpha}+\frac{\alpha}{1+\alpha}\parallel\boldsymbol{\sigma}\parallel^{1+\alpha}\right)\\&=\dot{\boldsymbol{\gamma}}^{\mathrm{T}}\mathrm{sig}^{2-\alpha}(\boldsymbol{\kappa})+\left(c_1c_2+\frac{c_1+c_3}{1+\alpha}\right)\parallel\boldsymbol{\kappa}\parallel^{1+\alpha}+\frac{c_1k_1}{1+\beta}\parallel\boldsymbol{\kappa}\parallel^{1+\beta}\\&\quad+\frac{c_3\alpha}{1+\alpha}\parallel\boldsymbol{\sigma}\parallel^{1+\alpha}+\frac{c_1k_1\beta}{1+\beta}\parallel\boldsymbol{\sigma}\parallel^{1+\beta}+\frac{c_1\alpha}{1+\alpha}\parallel\tilde{\boldsymbol{\nu}}\parallel^{1+\frac{1}{\alpha}}\end{aligned} \tag{40}$$

where $c_1=(2-\alpha)\,k_2^{\frac{1}{\alpha}}\lambda_{\max}(\boldsymbol{H})$, $c_2=2^{1-\alpha}(8n)^{\frac{1-\alpha}{2}}$, $c_3=c_1k_2(8n)^{\frac{1-\alpha}{2}}$.

Noting that $\boldsymbol{\gamma}_i=\boldsymbol{v}_i-\hat{\boldsymbol{v}}_i-\dot{\boldsymbol{\Delta}}_{i,0}+k_1\mathrm{sig}^{\beta}(\boldsymbol{\sigma}_i)$, we substitute $\boldsymbol{\gamma}_i$, Equation (4) and control scheme Equation (34) into the first term in the left hand of Equation (40) and we can get

$$\begin{aligned}&\dot{\boldsymbol{\gamma}}_i^{\mathrm{T}}\mathrm{sig}^{2-\alpha}(\boldsymbol{\kappa}_i)\\&=-\left[k_3\boldsymbol{\chi}(\boldsymbol{u}_i)\,\mathrm{sig}^{2\alpha-1}(\boldsymbol{\kappa}_i)+k_4\boldsymbol{\chi}(u_i)\,\mathrm{sig}^{\beta-1+\alpha}(\boldsymbol{\kappa}_i)\right]^{\mathrm{T}}\mathrm{sig}^{2-\alpha}(\boldsymbol{\kappa}_i)\\&\quad+\left[k_5\boldsymbol{\chi}(\boldsymbol{u}_i)\,\mathrm{sig}^{2-\alpha}(\boldsymbol{\kappa}_i)\right]^{\mathrm{T}}\mathrm{sig}^{2-\alpha}(\boldsymbol{\kappa}_i)\\&\quad+\left[\boldsymbol{F}_i+\boldsymbol{d}_i+\boldsymbol{g}(x_i)\boldsymbol{d}_{sqi}-\boldsymbol{\chi}(u_i)\,\frac{\|F_i\|^2\mathrm{sig}^{2-\alpha}(\boldsymbol{\kappa}_i)}{2\iota_f^2}\right]^{\mathrm{T}}\mathrm{sig}^{2-\alpha}(\boldsymbol{\kappa}_i)\\&\le-k_3\chi_{min}(1-\delta)\boldsymbol{\kappa}_i^{\mathrm{T}}\mathrm{sig}^{\alpha}(\boldsymbol{\kappa}_i)-k_4\boldsymbol{\chi}_{min}(1-\delta)\boldsymbol{\kappa}_i^{\mathrm{T}}\mathrm{sig}^{\beta}(\boldsymbol{\kappa}_i)-k_5\boldsymbol{\chi}_{min}(1-\delta)\|\boldsymbol{\kappa}_i\|^{4-2\alpha}\\&\quad-\chi_{min}(1-\delta)\frac{\|\boldsymbol{F}_i\|^2\|\boldsymbol{\kappa}_i\|^{4-2\alpha}}{2\iota_f}+|\boldsymbol{F}_i|^{\mathrm{T}}\left|\mathrm{sig}^{2-\alpha}(\boldsymbol{\kappa}_i)\right|+\left(\boldsymbol{d}_i+\boldsymbol{g}(\boldsymbol{x}_i)\boldsymbol{d}_{sqi}\right)^{\mathrm{T}}\left[\mathrm{sig}^{2-\alpha}(\boldsymbol{\kappa}_i)\right]\end{aligned}$$

https://doi.org/10.1017/aer.2023.23 Published online by Cambridge University Press

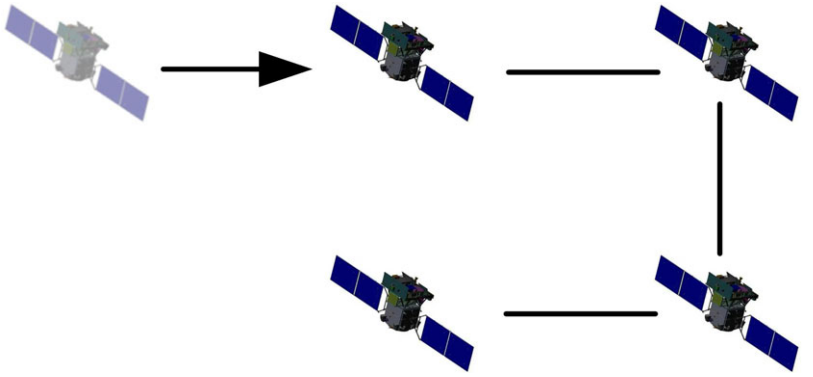

Figure 3. *Communication topology.*

$$\leq -k_3\chi_{min}(1-\delta)\,\boldsymbol{\kappa}_i{}^{\mathrm{T}}\mathrm{sig}^{\alpha}(\boldsymbol{\kappa}_i) - k_4\chi_{min}(1-\delta)\,\boldsymbol{\kappa}_i{}^{\mathrm{T}}\mathrm{sig}^{\beta}(\boldsymbol{\kappa}_i) + \frac{\iota_f}{2\chi_{min}(1-\delta)} + \frac{d_{\max}^2 + 8(g_{max}u_{\min})^2}{2\iota_d} \tag{41}$$

where the inequality $|\boldsymbol{F}_i|^{\mathrm{T}}\left|\mathrm{sig}^{2-\alpha}(\boldsymbol{\kappa}_i)\right| \leq \chi_{min}(1-\delta)\,\frac{\|\boldsymbol{F}_i\|^2\|\boldsymbol{\kappa}_i\|^{4-2\alpha}}{2\iota_f} + \frac{\iota_f}{2\chi_{min}(1-\delta)}$ and **Assumption 2** have been used.

Noting that $\dot{\boldsymbol{\gamma}}^{\mathrm{T}}\mathrm{sig}^{2-\alpha}(\boldsymbol{\kappa}) = \sum_{i=1}^{n}\dot{\boldsymbol{\gamma}}_i^{\mathrm{T}}\mathrm{sig}^{2-\alpha}(\kappa_i)$, we can rewrite Equation (40) as

$$\begin{aligned}\dot{V}_2 \leq & -\left[k_3\chi_{min}(1-\delta) - c_1c_2 - \frac{c_1+c_3}{1+\alpha}\right]\|\boldsymbol{\kappa}\|^{1+\alpha} \\ & -\left[k_4\chi_{min}(1-\delta)(8n)^{\frac{1+\beta}{2}} - \frac{c_1k_1}{1+\beta}\right]\|\boldsymbol{\kappa}\|^{1+\beta} \\ & + \frac{c_3\alpha}{1+\alpha}\|\boldsymbol{\sigma}\|^{1+\alpha} + \frac{c_1k_1\beta}{1+\beta}\|\boldsymbol{\sigma}\|^{1+\beta} + \frac{c_1\alpha}{1+\alpha}\|\tilde{\boldsymbol{\nu}}\|^{1+\frac{1}{\alpha}} \\ & + \frac{n\iota_f}{2\chi_{min}(1-\delta)} + \frac{nd_{\max}^2 + 8n(g_{max}u_{\min})^2}{2\iota_d}\end{aligned} \tag{42}$$

Consider the overall Lyapunov function $V = V_{\zeta 1} + V_1 + V_2$ and the time derivative of V is given by the sum of Equation (17), Equation (33) and Equation (42).

$$\begin{aligned}\dot{V} \leq & -p_{\sigma\beta}\|\boldsymbol{\sigma}\|^{1+\beta} - p_{\sigma\alpha}\|\boldsymbol{\sigma}\|^{1+\alpha} - p_{\kappa\beta}\|\boldsymbol{\kappa}\|^{1+\beta} - p_{\kappa\alpha}\|\boldsymbol{\kappa}\|^{1+\alpha} \\ & - p_{\zeta\beta}\|\boldsymbol{\zeta}\|^{1+\beta} - p_{\zeta\alpha}\|\boldsymbol{\zeta}\|^{1+\alpha} - p_{\zeta}\|\boldsymbol{\zeta}\|^{1+\frac{1}{\alpha}} + p_b \\ \leq & -l_{\alpha}\left(\|\boldsymbol{\zeta}\|^2 + \|\boldsymbol{\sigma}\|^2 + \|\boldsymbol{\kappa}\|^2\right)^{\frac{1+\alpha}{2}} - l_{\beta}\left(\|\boldsymbol{\zeta}\|^2 + \|\boldsymbol{\sigma}\|^2 + \|\boldsymbol{\kappa}\|^2\right)^{\frac{1+\beta}{2}} + p_b\end{aligned} \tag{43}$$

where $p_{\sigma\beta} = k_1 - \frac{c_1k_1\beta}{1+\beta}$, $p_{\sigma\alpha} = k_2 - \frac{1+2^{1-\alpha}}{1+\alpha} - \frac{c_3\alpha}{1+\alpha}$, $p_{\kappa\beta} = k_4\chi_{min}(1-\delta)(8n)^{\frac{1+\beta}{2}} - \frac{c_1k_1}{1+\beta}$, $p_{\kappa\alpha} = k_3\chi_{min}(1-\delta) - c_1c_2 - \frac{c_1+c_3}{1+\alpha} - \frac{2^{1-\alpha}\alpha}{1+\alpha}$, $p_{\zeta\beta} = o_2(1-\iota)(8n)^{\frac{1-\beta}{2}}$, $p_{\zeta\alpha} = o_3(1-\iota)$, $p_{\zeta} = o_1(1-\iota)(8n)^{\frac{\alpha-1}{2\alpha}} - \frac{(c_1+1)\alpha}{(1+\alpha)\lambda_{\min}(H)^{1+\frac{1}{\alpha}}}$, $p_b = \frac{n\iota_f}{2\chi_{min}(1-\delta)} + \frac{nd_{\max}^2+8n(g_{max}u_{\min})^2}{2\iota_d} + \frac{o_4(1-\iota)\delta k}{4}$, $l_{\alpha} = \max\left(p_{\sigma\alpha}, p_{\kappa\alpha}, p_{\zeta\alpha}\right)$, $l_{\beta} = \max\left(p_{\sigma\beta}, p_{\kappa\beta}, p_{\zeta\beta}\right)$ are positive constants.

https://doi.org/10.1017/aer.2023.23 Published online by Cambridge University Press

Table 1. *Initial orbital elements of the virtual leader*

Orbit elements	Value
Semi major axis/km	6878.137
Eccentricity	0
Inclination/deg	42
Right ascension of the ascending node/deg	50
Argument of latitude/deg	20
Initial value of True anomaly during simulation/deg	0

Table 2. *Desired states of each follower spacecraft*

Desired states		Spacecraft 1	Spacecraft 2	Spacecraft 3	Spacecraft 4
Desired position	$\vec{r}_i$-$\vec{r}_0$	$\begin{bmatrix}200 & 0 & 0\end{bmatrix}^{\mathrm{T}}$	$\begin{bmatrix}400 & 0 & 0\end{bmatrix}^{\mathrm{T}}$	$\begin{bmatrix}600 & 0 & 0\end{bmatrix}^{\mathrm{T}}$	$\begin{bmatrix}800 & 0 & 0\end{bmatrix}^{\mathrm{T}}$
	$\dot{\vec{r}}_i$-$\dot{\vec{r}}_0$	$\begin{bmatrix}0 & 0 & 0\end{bmatrix}^{\mathrm{T}}$	$\begin{bmatrix}0 & 0 & 0\end{bmatrix}^{\mathrm{T}}$	$\begin{bmatrix}0 & 0 & 0\end{bmatrix}^{\mathrm{T}}$	$\begin{bmatrix}0 & 0 & 0\end{bmatrix}^{\mathrm{T}}$
Desired attitude	$\boldsymbol{q}_i$	$\begin{bmatrix}1 & 0 & 0 & 0\end{bmatrix}^{\mathrm{T}}$	$\begin{bmatrix}1 & 0 & 0 & 0\end{bmatrix}^{\mathrm{T}}$	$\begin{bmatrix}1 & 0 & 0 & 0\end{bmatrix}^{\mathrm{T}}$	$\begin{bmatrix}1 & 0 & 0 & 0\end{bmatrix}^{\mathrm{T}}$
	$\vec{\boldsymbol{\omega}}_i$	$\begin{bmatrix}0 & 0 & 0\end{bmatrix}^{\mathrm{T}}$	$\begin{bmatrix}0 & 0 & 0\end{bmatrix}^{\mathrm{T}}$	$\begin{bmatrix}0 & 0 & 0\end{bmatrix}^{\mathrm{T}}$	$\begin{bmatrix}0 & 0 & 0\end{bmatrix}^{\mathrm{T}}$

Similar to the method used in Equation (38), we can derive that $V_2 \leq 2^{1-\alpha} \| \boldsymbol{\kappa} \|^2$. Then, $V = V_{**\zeta 1} + V_1 + V_2$ can be rewritten as

$$\begin{aligned} V &\leq \frac{1}{2\lambda_{\min}(\boldsymbol{H})} \| \boldsymbol{\zeta} \|^2 + \frac{1}{2\lambda_{\max}(\boldsymbol{H})} \| \boldsymbol{\sigma} \|^2 + 2^{1-\alpha} \| \boldsymbol{\kappa} \|^2 \\ &\leq l\left(\| \boldsymbol{\zeta} \|^2 + \| \boldsymbol{\sigma} \|^2 + \| \boldsymbol{\kappa} \|^2 \right) \end{aligned} \tag{44}$$

where $l = \max\left(\frac{1}{2\lambda_{\min}(\boldsymbol{H})}, 2^{1-\alpha} \right)$. Substituting Equation (44) into Equation (43), it can yield

$$\dot{V} \leq -\frac{l_\alpha}{l^{\frac{1+\alpha}{2}}} V^{\frac{1+\alpha}{2}} - \frac{l_\beta}{l^{\frac{1+\beta}{2}}} V^{\frac{1+\beta}{2}} + p_b \tag{45}$$

By using **Lemma 1**, we can conclude that $\boldsymbol{\sigma}$ and $\boldsymbol{\kappa}$ converge to a region within fixed time $T_2 \leq 1/\left[\frac{l_\alpha}{l^{\frac{1+\alpha}{2}}} \left(1 - \frac{1+\alpha}{2} \right) \right] + 1/\left[\frac{l_\beta}{l^{\frac{1+\beta}{2}}} \left(\frac{1+\beta}{2} - 1 \right) \right]$, which in turn implies that $\boldsymbol{\gamma}$ and $\boldsymbol{\gamma}_d$ converge to zero within fixed time as well. Since $\boldsymbol{\sigma} = \boldsymbol{H}\boldsymbol{e}_x$ and $\boldsymbol{e}_v = \boldsymbol{\gamma} - \boldsymbol{\gamma}_d + \tilde{\boldsymbol{\nu}} - k_1 \mathrm{sig}^\beta(\boldsymbol{\sigma}) - k_2 \mathrm{sig}^\alpha(\boldsymbol{\sigma})$, we can obtain that the tracking errors $\boldsymbol{e}_x$ and $\boldsymbol{e}_v$ converge to the origin within fixed time. □

Remark 8. It should be mentioned that Equation (8) is inspired by [39], which only achieved an asymptotic convergence result. In contrast, we deal with the actuator saturation and input quantisation problems under the framework of the "adding a power integrator" technique in an ingenious way, by embedding $-\frac{\|\boldsymbol{F}_i\|^2 \mathrm{sig}^{2-\alpha}(\boldsymbol{\kappa}_i)}{2\iota_f}$ in Equation (34).

Remark 9. Recalling the time derivative of V_1 in Equation (33), it is noted that $\frac{\alpha}{1+\alpha} \| \tilde{\boldsymbol{\nu}} \|^{1+\frac{1}{\alpha}}$ would be compensated by $-o_1(1-\iota)(8n)^{\frac{\alpha-1}{2\alpha}} \| \boldsymbol{\zeta} \|^{1+\frac{1}{\alpha}}$ in Equation (17), which is generated by the nonlinear term $-o_1 \mathrm{sig}^{\frac{1}{\alpha}}\left[\boldsymbol{\zeta}_i(t_k) \right]$ in Equation (9). By doing so, we guarantee the fixed time stability of the entire closed-loop system without recourse to the separation principle.

4.0 Numerical simulations and results

The performance of the proposed observer Equation (9), Equation (24) and the control scheme Equation (34) are tested in Numerical simulations. Four spacecrafts together with

https://doi.org/10.1017/aer.2023.23 Published online by Cambridge University Press

Table 3. *Initial states of each follower spacecraft*

Initial states		Spacecraft 1	Spacecraft 2	Spacecraft 3	Spacecraft 4
Initial position	$\vec{r}_i(0)$-$\vec{r}_0(0)$	$[-7.5 \quad 5 \quad -9]^{\mathrm{T}}$	$[-10 \quad 6 \quad 7.5]^{\mathrm{T}}$	$[8 \quad 9 \quad -6.5]^{\mathrm{T}}$	$[10 \quad -5 \quad 6]^{\mathrm{T}}$
	$\dot{\vec{r}}_i(0)$-$\dot{\vec{r}}_0(0)$	$[0 \quad 0 \quad 0]^{\mathrm{T}}$	$[0 \quad 0 \quad 0]^{\mathrm{T}}$	$[0 \quad 0 \quad 0]^{\mathrm{T}}$	$[0 \quad 0 \quad 0]^{\mathrm{T}}$
Initial attitude	$\boldsymbol{q}_i(0)$	$\begin{bmatrix} 0.8361 \\ 0.3188 \\ 0.3296 \\ -0.3011 \end{bmatrix}$	$\begin{bmatrix} 0.9296 \\ -0.3267 \\ -0.1702 \\ 0.01137 \end{bmatrix}$	$\begin{bmatrix} 0.7636 \\ -0.459 \\ -0.217 \\ 0.377 \end{bmatrix}$	$\begin{bmatrix} 0.9681 \\ -0.009799 \\ 0.08571 \\ 0.2142 \end{bmatrix}$
	$\boldsymbol{\theta}_i(0)$	$[-26 \quad 48 \quad 30]^{\mathrm{T}}$	$[8 \quad -18 \quad -40]^{\mathrm{T}}$	$[54 \quad 2 \quad -61]^{\mathrm{T}}$	$[24 \quad 12 \quad -9]^{\mathrm{T}}$
	$\vec{\boldsymbol{\omega}}_i(0)$	$[0 \quad 0 \quad 0]^{\mathrm{T}}$	$[0 \quad 0 \quad 0]^{\mathrm{T}}$	$[0 \quad 0 \quad 0]^{\mathrm{T}}$	$[0 \quad 0 \quad 0]^{\mathrm{T}}$
Initial estimation	$\hat{\boldsymbol{r}}_i(0)$-$\vec{r}_0(0)$	$[200-7.5 \quad 5 \quad -9]^{\mathrm{T}}$	$[400-10 \quad 6 \quad 7.5]^{\mathrm{T}}$	$[600+8 \quad 9 \quad -6.5]^{\mathrm{T}}$	$[800+10 \quad -5 \quad 6]^{\mathrm{T}}$
	$\dot{\hat{\boldsymbol{r}}}_i(0)$-$\dot{\vec{r}}_0(0)$	$[0 \quad 0 \quad 0]^{\mathrm{T}}$	$[0 \quad 0 \quad 0]^{\mathrm{T}}$	$[0 \quad 0 \quad 0]^{\mathrm{T}}$	$[0 \quad 0 \quad 0]^{\mathrm{T}}$
	$\hat{\boldsymbol{\theta}}_{i,0}(0)$	$[-26 \quad 48 \quad 30]^{\mathrm{T}}$	$[8 \quad -18 \quad -40]^{\mathrm{T}}$	$[54 \quad 2 \quad -61]^{\mathrm{T}}$	$[24 \quad 12 \quad -9]^{\mathrm{T}}$
	$\hat{\boldsymbol{\omega}}_{i,0}(0)$	$[0 \quad 0 \quad 0]^{\mathrm{T}}$	$[0 \quad 0 \quad 0]^{\mathrm{T}}$	$[0 \quad 0 \quad 0]^{\mathrm{T}}$	$[0 \quad 0 \quad 0]^{\mathrm{T}}$

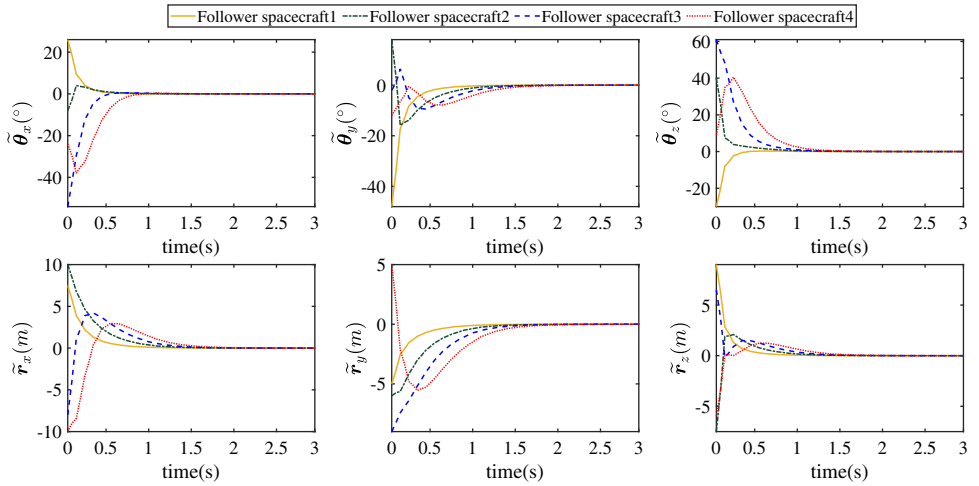

Figure 4. *Errors of observation.*

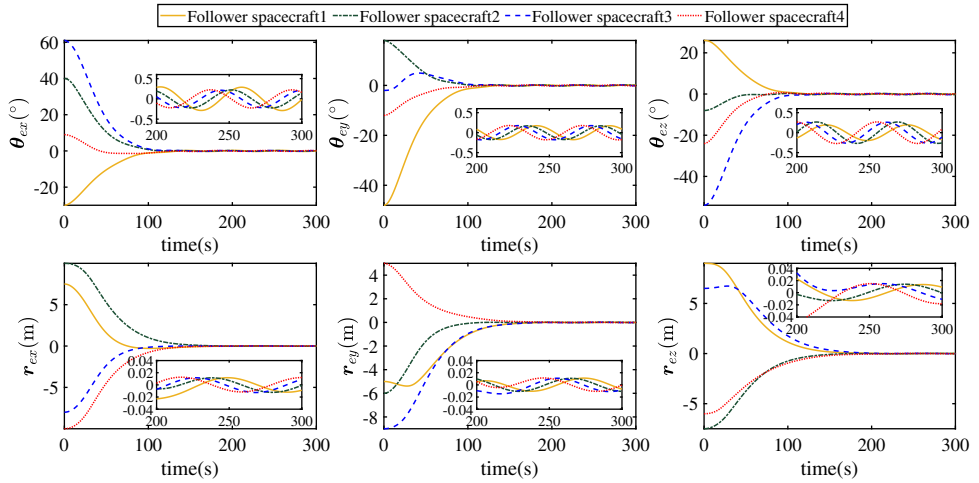

Figure 5. *Errors of attitude and position.*

one virtual leader are considered, as shown in Fig. 3. The adjacency matrix A is set as [0, 0.1, 0, 0; 0.1, 0, 0.1, 0; 0, 0.1, 0, 0.1; 0, 0, 0.1, 0].

Statistics show that approximately 73% of SFF missions operate in low Earth orbit (LEO), and the vast majority of SFF missions are executed by small spacecraft with a mass of less than 500 kg [25]. The simulation environment is therefore set up, so that spacecraft with a mass of about 100 kg follow the virtual leader in LEO. For follower spacecrafts, the mass are chosen as $m_1 = 102$kg, $m_2 = 104$kg, $m_3 = 103$kg, $m_4 = 99$kg and the inertia matrices are chosen as $\boldsymbol{J}_1 = [15.2, -0.04, 0.05; -0.04, 17.3, 0.02; 0.05, 0.02, 19.5]$, $\boldsymbol{J}_2 = [14.7, 0.01, -0.06; 0.01, 17.3, 0.03; -0.06, 0.03, 19.5]$, $\boldsymbol{J}_3 = [15.4, -0.043, 0; 0.03, 17.1, 0.01; 0, 0.01, 20.7]$, $\boldsymbol{J}_4 = [14.9, -0.04, 0; -0.04, 16.9, 0.02; 0, 0.02, 19.8]$. The external disturbances are selected as $\boldsymbol{f}_{ip} = 0.01[0.9\sin(0.075t + 0.8i - 0.3), 1\sin(0.09t + 0.8i + 0.8), 1.1\sin(0.06t + 0.8i + 0.2)]^T N$ and $\boldsymbol{\tau}_{ip} = 0.001[0.9\sin(0.11t + 0.8i + 0.2), 1\sin(0.125t + 0.8i + 1.2), 1.1\sin(0.1125t + 0.8i + 2.2)]^T N \cdot m$. Table 1 gives the virtual leader's initial orbital elements.

https://doi.org/10.1017/aer.2023.23 Published online by Cambridge University Press

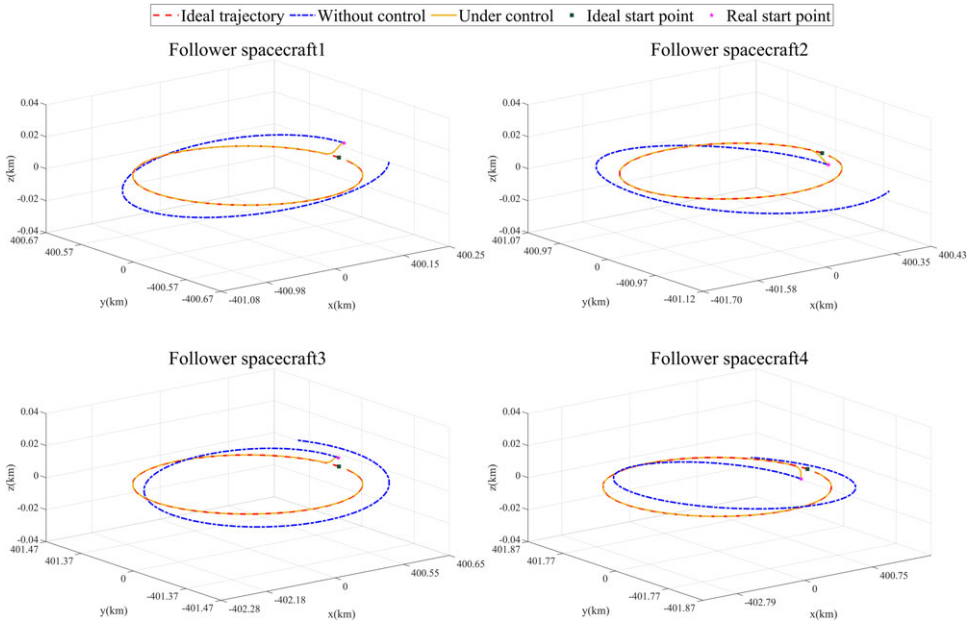

Figure 6. *Control of the orbit.*

The controller and observer parameters of the ith follower spacecraft are chosen as $\alpha = 0.9$, $\beta = 2$, $o_1 = 0.5$, $o_2 = 0.5$, $o_3 = 0.005$, $o_4 = 100$, $k_{o1} = 0.0012$, $k_{o2} = 7.8240$, $k_{o3} = 3$, $\iota = 0.1$, $\delta_o = 0.001$, $k_1 = 1$, $k_2 = 0.05$, $k_3 = 0.1$, $k_4 = 0.5$, $k_5 = 0.5$. The dead zone of the control force and the control torque are $0.005N$ and $0.0004N \cdot m$, quantified density $\delta = 0.2$. As shown in Table 2, we expect each spacecraft to be 200m from the others and to have the same attitude. $\vec{\boldsymbol{r}}_0$ represents the virtual leader's position vector. $\vec{\boldsymbol{r}}_i - \vec{\boldsymbol{r}}_0$ denotes the position deviation for ith follower spacecraft from the virtual leader. Besides, Table 3 shows the initial states of each spacecraft. In order to describe the attitude more intuitively, we have used Euler angles $\boldsymbol{\theta}_i(0)$ and $\boldsymbol{\theta}_i(t)$ in the initial settings and the subsequent simulation figures. It is worth pointing out that we still use the dual quaternion in the control algorithm, where the Euler angles are used only to express the attitude change intuitively. The observer's estimated initial value for the ith follower spacecraft is taken as its initial state value.

4.1 Evaluation of control performance and convergence

To display the observation errors intuitively, we depict $\widetilde{\boldsymbol{q}}_i, \widetilde{\boldsymbol{r}}_i$ in Fig. 4 instead of $\widetilde{\boldsymbol{v}}_i$, where $\widetilde{\boldsymbol{q}}_i$ and $\widetilde{\boldsymbol{r}}_i$ are observation errors of the virtual leader's vector quaternion and position. It can be observed that all follower spacecrafts can estimate the virtual leader's velocity in a fixed time.

The time responses of the attitude quaternion and position tracking errors $\boldsymbol{\theta}_e, \boldsymbol{r}_e$ of each follower spacecraft are given in Fig. 5. The trajectory of the spacecraft's position in the uncontrolled and the controlled case during an orbital period of 5,578 seconds is shown in Fig. 6. It is important to note that Fig. 6 uses an inhomogeneous coordinate system for more visual comparison. In addition, the minimum value, maximum value, and standard deviation of the controller convergence errors from 250 to 300 seconds are explicitly described in Table 4, which is needed while implementing the engineering solution of the mathematical treatment.

Figure 7 illustrate the control force and the control torque bounded by $0.52N$ and $0.02N \cdot m$. As shown in these figures, the control output in the initial stage is saturated. Obviously, even in the presence of actuator saturation and input quantisation, the SFF system can estimate the states of the virtual

https://doi.org/10.1017/aer.2023.23 Published online by Cambridge University Press

Table 4. *Desired states of each follower spacecraft*

		Minimum value	Maximum value	Standard deviation
#1	$\boldsymbol{\theta}_{ex}, \boldsymbol{r}_{ex}$	−0.2883°, −0.0231m	0.2957°, 0.0118m	0.2066°, 0.0106m
	$\boldsymbol{\theta}_{ey}, \boldsymbol{r}_{ey}$	−0.1753°, −0.0104m	0.1732°, 0.0111m	0.1224°, 0.0069m
	$\boldsymbol{\theta}_{ez}, \boldsymbol{r}_{ez}$	−0.1976°, −0.0129m	0.1952°, 0.0231m	0.1315°, 0.0102m
#2	$\boldsymbol{\theta}_{ex}, \boldsymbol{r}_{ex}$	−0.2235°, −0.0123m	0.2209°, 0.0116m	0.1486°, 0.0080m
	$\boldsymbol{\theta}_{ey}, \boldsymbol{r}_{ey}$	−0.1733°, −0.0107m	0.1701°, 0.0108m	0.1216°, 0.0074m
	$\boldsymbol{\theta}_{ez}, \boldsymbol{r}_{ez}$	−0.2684°, −0.0130m	0.2659°, 0.0140m	0.1910°, 0.0097m
#3	$\boldsymbol{\theta}_{ex}, \boldsymbol{r}_{ex}$	−0.2149°, −0.0126m	0.2130°, 0.0116m	0.1484°, 0.0081m
	$\boldsymbol{\theta}_{ey}, \boldsymbol{r}_{ey}$	−0.1795°, −0.0147m	0.1754°, 0.0109m	0.1249°, 0.0088m
	$\boldsymbol{\theta}_{ez}, \boldsymbol{r}_{ez}$	−0.2617°, −0.0108m	0.2618°, 0.0327m	0.1918°, 0.0081m
#4	$\boldsymbol{\theta}_{ex}, \boldsymbol{r}_{ex}$	−0.2247°, −0.0116m	0.2245°, 0.0126m	0.1638°, 0.0085m
	$\boldsymbol{\theta}_{ey}, \boldsymbol{r}_{ey}$	−0.1798°, −0.0107m	0.1780°, 0.0113m	0.1259°, 0.0069m
	$\boldsymbol{\theta}_{ez}, \boldsymbol{r}_{ez}$	−0.2723°, −0.0501m	0.2677°, 0.0149m	0.1857°, 0.0177m

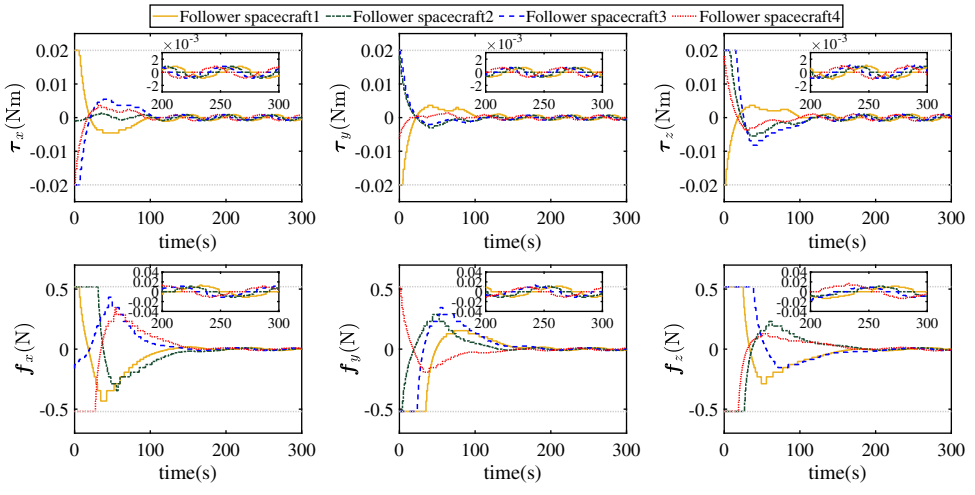

Figure 7. *Control torque and force.*

leader effectively and track the trajectory of the virtual leader while maintaining the desired formation configuration.

4.2 Comparison

To highlight the advantages of the proposed triggering condition Equation (24), we use the trigger conditions in [17] as a comparison, which can be expressed as

$$g_{ij}(t) = \int_{t_k}^{t} \eta_1 h_{\max} \left| \eta_{2ij}(t_k) + B_3 \right| \mathrm{d}s - \frac{\iota}{1+\iota} \left| \dot{\hat{v}}_{ij}(t_k) + \frac{k_{o4}}{\iota} \right| \tag{46}$$

where k_{o4} is positive parameter. Meanwhile, to obtain a fair comparison, take the two cases of $k_{o4} = k_{o1}\sqrt{e}$ and $k_{o4} = k_{o1}\sqrt{e^{1+k_{o2}}}$ for comparison, where $k_{o1}\sqrt{e}$ and $k_{o1}\sqrt{e^{1+k_{o2}}}$ are the upper and lower bounds of the

https://doi.org/10.1017/aer.2023.23 Published online by Cambridge University Press

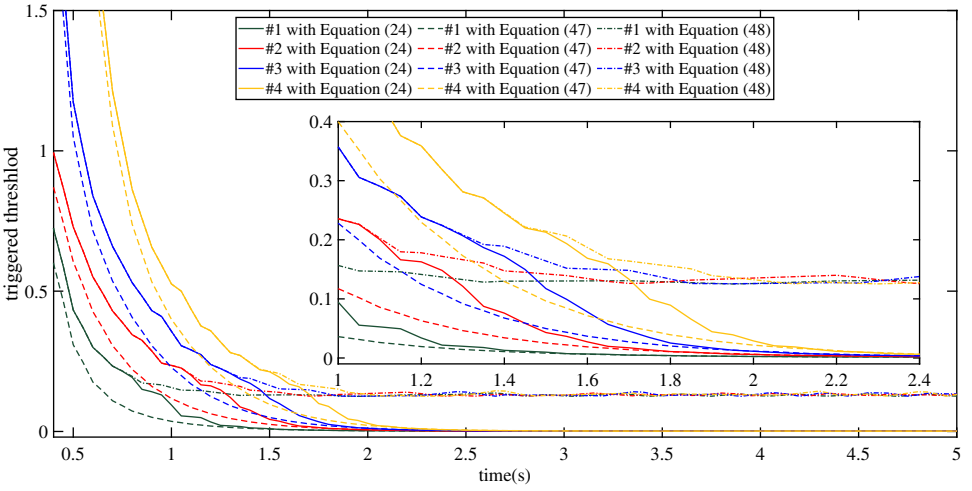

Figure 8. *Curves of triggering condition thresholds.*

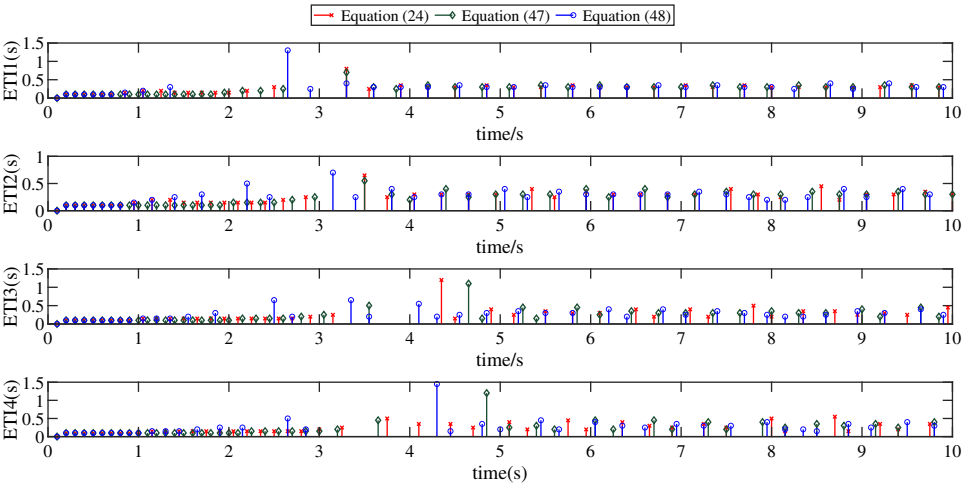

Figure 9. *Curves of triggering condition thresholds.*

nonlinear term $k_{o1}\sqrt{e^{1+k_{o2}\tanh\left(k_{o3}\left|\xi_{ij}(t_k)\right|\right)}}$ in Equation (24), respectively. The two cases are expressed as

$$g_{ij}(t)=\int_{t_k}^{t}\eta_1 h_{\max}\left|\eta_{2ij}(t_k)+B_3\right|\mathrm{d}s-\frac{\iota}{1+\iota}\left|\dot{\hat{v}}_{ij}(t_k)+\frac{k_{o1}}{\iota}\sqrt{e}\right| \tag{47}$$

$$g_{ij}(t)=\int_{t_k}^{t}\eta_1 h_{\max}\left|\eta_{2ij}(t_k)+B_3\right|\mathrm{d}s-\frac{\iota}{1+\iota}\left|\dot{\hat{v}}_{ij}(t_k)+\frac{k_{o1}}{\iota}\sqrt{e^{1+k_{o2}}}\right| \tag{48}$$

According to the statistical analysis of the trigger simulation data, Figs. (8)–(9) can be obtained. Figure (8) plots the comparison results of the trigger threshold. The triggering intervals of the SFF system is presented in Fig. (9).

We divide the convergence process of the observation errors into the transient-state phase and the steady-state phase for discussion, aiming to demonstrate the superiority of the proposed ETM in detail. (A). In the transient-state phase. Equation (24) has a larger trigger threshold than Equation (47), but almost the same as Equation (48). Hence, the trigger times of Equation (24) is in the middle of the trigger

https://doi.org/10.1017/aer.2023.23 Published online by Cambridge University Press

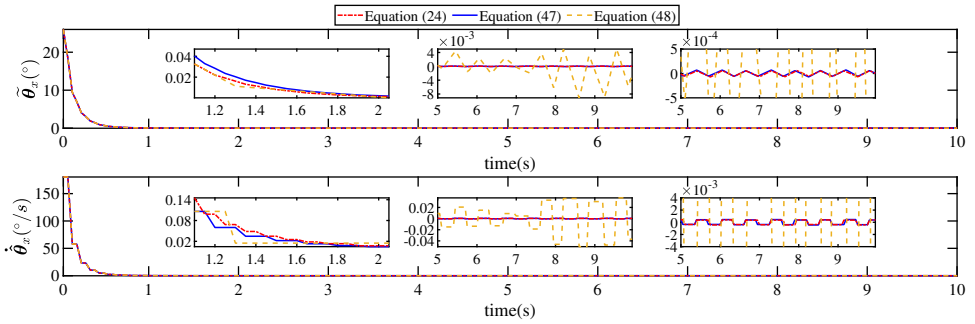

Figure 10. *Comparison of observer performance under different ETMs.*

times of Equation (47) and Equation (48). (B). In the steady-state phase. Equation (24) has a smaller trigger threshold than Equation (48), but almost the same as Equation (47). Therefore, the trigger times of Equation (24) and Equation (47) are almost the same. Further, The norm distribution of the observation errors of Equation (24) and Equation (47) are almost the same.

As can be observed in these discussions and figures, Equation (24) achieves the same steady-state performance as Equation (47) with less communication penalty. It is because that the lower limit of the trigger threshold of Equation (24) fluctuates with the accuracy compared with the stable lower limit of the trigger threshold of Equation (46). In other words, Equation (24) realises the amplification of the lower limit of trigger threshold when the error is large and the reduction of the lower limit of trigger threshold when the error is small, that is the proposed ETM achieves the same steady-state performance with less communication penalty.

However, there is no win-win situation in control systems. In fact, although Equation (24) has reduced communication penalty compared to Equation (47), it has increased fuel consumption. Figure (10) illustrates this with an example $\widetilde{\boldsymbol{\theta}}_x$ and $\dot{\hat{\boldsymbol{\theta}}}_x$ of the follower spacecraft 1. For an observer, the fuel it consumes is its control input $\dot{\hat{\boldsymbol{\theta}}}_x$. The quantitative analysis of the different ETMs is given in Table 5, where errors distribution denotes the range of $\sum_{i=1}^{4}\sum_{j=1}^{6}|z_{ij}|/24$ with observer error z_{ij}, and total input denotes $\sum_{i=1}^{4}\sum_{j=1}^{6}\int ou_{ij}(t)$ with observer control input ou_{ij}. It can be calculated that ETM Equation (24) achieves a 8.98% saving in communication resources at a cost of 2.62% fuel consumption compared to ETM Equation (47).

Remark 10. It should be noted that the execution of the observer is fully digital and does not really require the consumption of fuel, which is why fuel is quoted in the text above. In other words, the application of the ETM in the observer designed in this paper circumvents the cost of its fuel consumption.

Please note that ETM is only embedded in the observer and is not mounted on the controller. Figure (11) illustrates the impact of different ETMs on the controller's performance with an example $\boldsymbol{\theta}_{ex}$ of the follower spacecraft 1. It can be seen that the observer embedding different ETMs has no effect on the transient performance of the controller, which is due to the fact that the observer converges much faster than the controller converges. Equation (24) and (47) have the same effect on the steady-state performance of the controller, and Equation (48) causes the steady-state performance of the controller to deteriorate. This is because the observation error of Equation (48) is higher than that of Equation (24) and Equation (47) (as shown in Fig. 10), and the observation error affects the convergence error of the controller.

Besides, to emphasise the advantages of the proposed control scheme, we reproduced the asymptotic controller [40] and the finite-time controller [41] in numerical simulations for comparison. We consider two performance indices for an intuitive comparison: (A) The Attitude Station-Keeping Absolute Error

https://doi.org/10.1017/aer.2023.23 Published online by Cambridge University Press

Table 5. *Communication analysis of different ETMs for all spacecrafts in 10 seconds*

	Total trigger times	Errors distribution $(e-4)$	Total input
Equation (24)	167	$[-0.8475, 0.8364]$	653.5
Equation (47)	182	$[-0.8503, 0.8421]$	636.8
Equation (48)	148	$[-83.5347, 84.3176]$	1513.0

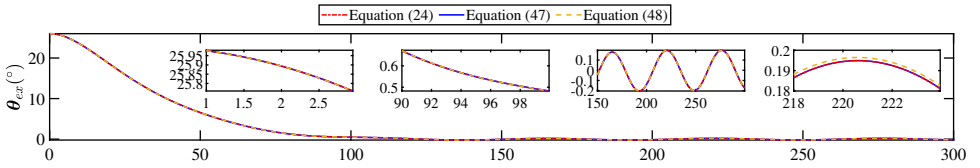

Figure 11. *Impact of different ETMs on the controller's performance.*

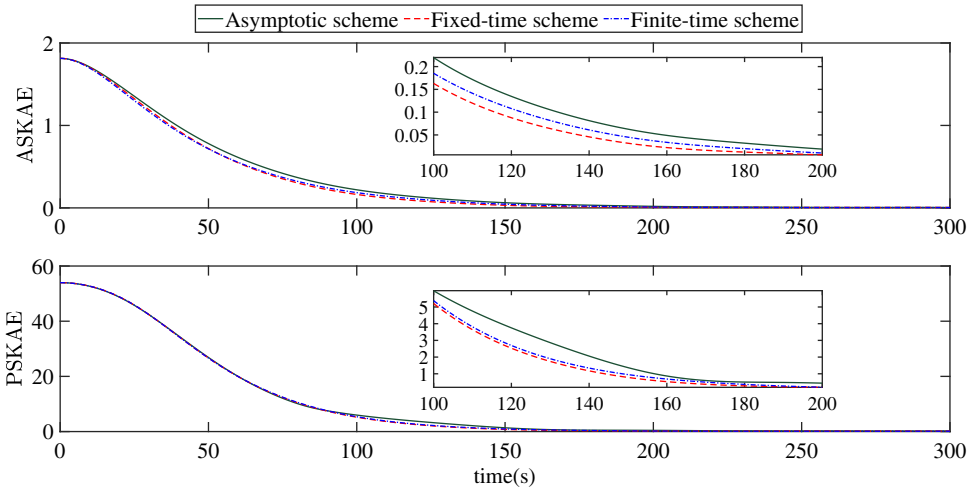

Figure 12. *The comparison curves of the two performance indicators.*

(ASKAE) $\sum_{i=1}^{n} \|\boldsymbol{q}_{e,i}\|$. (B) The Position Station-Keeping Absolute Error (PSKAE) $\sum_{i=1}^{n} \|\boldsymbol{r}_{e,i}\|$. Figure 12 gives the two performance indicators' comparison curves for each control scheme. Obviously, the proposed fixed time controllers demonstrate faster convergence rates in both performance indices.

5.0 Conclusion

This paper investigated the attitude and position coupled tracking control problem of SFF systems with actuator saturation and input quantisation under an undirected communication graph. Since the communication bandwidth is limited, a resource-saving distributed control scheme was developed based on an event-triggered observer and the adding a power integrator technique. It is worth remarking that the novel observer realised the amplification of the trigger threshold when the error is large, but neither increased the convergence time nor affected the final accuracy. Besides, the control scheme compensated the actuator saturation and input quantisation in an ingenious way. Finally, a simulation of a four-spacecraft on LEO is carried out to illustrate the successful application of the proposed distributed control algorithm.

https://doi.org/10.1017/aer.2023.23 Published online by Cambridge University Press

The control scheme subject to the limited communication under the directed graph will be investigated in our future work.

Acknowledgements. This work was supported in part by the National Natural Science Foundation of China (grant number: 61304108) and National Key R&D Program of China (grant number: 2020YFC2200600).

Data availability. The data used to support the findings of this study are available from the corresponding author upon request.

Conflicts of interest. The authors declare that they have no known competing financial interests or personal relationships that could have appeared to influence the work reported in this paper.

References

[1] Mauro, G., Spiller, D., Bevilacqua, R. and D'Amico, S. Spacecraft formation flying reconfiguration with extended and impulsive maneuvers, *J. Franklin Inst.*, 2019, **356**, (6), pp 3474–3507.
[2] Shaw, G.B., Miller, D.W. and Hastings, D.E. Generalized characteristics of communication, sensing, and navigation satellite systems, *J. Spacecr. Rockets*, 2000, **37**, (6), pp 801–811.
[3] Ren, W. and Beard, R.W. Decentralized scheme for spacecraft formation flying via the virtual structure approach, *J. Guid. Control Dyn.*, 2004, **27**, (1), pp 73–82.
[4] Ahn, C. and Kim, Y. Point targeting of multisatellites via a virtual structure formation flight scheme, *J. Guid. Control Dyn.*, 2009, **32**, (4), pp 1330–1344.
[5] Jiakang, Z.H.O.U., Guangfu, M.A. and Qinglei, H.U. Delay depending decentralized adaptive attitude synchronization tracking control of spacecraft formation, *Chinese J. Aeronaut.*, 2012, **25**, (3), pp 406–415.
[6] Wu, B., Wang, D. and Poh, E.K. Decentralized sliding-mode control for spacecraft attitude synchronization under actuator failures, *Acta Astronaut.*, 2014, **105**, (1), pp 333–343.
[7] Zhou, J., Hu, Q. and Friswell, M.I. Decentralized finite time attitude synchronization control of satellite formation flying, *J. Guid. Control Dyn.*, 2013, **36**, (1), pp 185–195.
[8] Zou, A. and Kumar, K.D. Distributed attitude coordination control for spacecraft formation flying, *IEEE Trans. Aerosp. Electron. Syst.*, 2012, **48**, (2), pp 1329–1346.
[9] Zou, A., de Ruiter, A.H.J. and Kumar, K.D. Distributed finite-time velocity-free attitude coordination control for spacecraft formations, *Automatica*, 2016, **67**, pp 46–53.
[10] Polyakov, A. Nonlinear feedback design for fixed-time stabilization of linear control systems, *IEEE Trans. Autom. Control*, 2012, **57**, (8), pp 2106–2110.
[11] Ren, W. Formation keeping and attitude alignment for multiple spacecraft through local interactions, *J. Guid. Control Dyn.*, 2007, **30**, (2), pp 633–638.
[12] Han, G.A.O., Yuanqing, X.I.A., Zhang, X. and Zhang, G. Distributed fixed-time attitude coordinated control for multiple spacecraft with actuator saturation, *Chinese J. Aeronaut.*, 2022, **35**, (4), pp 292–302.
[13] Tabuada, P. Event-triggered real-time scheduling of stabilizing control tasks, *IEEE Trans. Autom. Control*, 2007, **52**, (9), pp 1680–1685.
[14] Dimarogonas, D.V., Frazzoli, E. and Johansson, K.H. Distributed event-triggered control for multi-agent systems, *IEEE Tran. Autom. Control*, 2012, **57**, (5), pp 1291–1297.
[15] Nowzari, C., Garcia, E. and Cortés, J. Event-triggered communication and control of networked systems for multi-agent consensus, *Automatica*, 2019, **105**, pp 1–27.
[16] Garcia, E., Cao, Y. and Casbeer, D.W. Periodic event-triggered synchronization of linear multi-agent systems with communication delays, *IEEE Trans. Autom. Control*, 2017, **62**, (1), pp 366–371.
[17] Liu, J., Zhang, Y., Yu, Y. and Sun, C. Fixed-time event-triggered consensus for nonlinear multiagent systems without continuous communications, *IEEE Trans. Syst. Man Cybern. Syst.*, 2019, **49**, (11), pp 2221–2229.
[18] Proskurnikov, A.V. and Mazo, M. Lyapunov event-triggered stabilization with a known convergence rate, *IEEE Trans. Autom. Control*, 2020, **65**, (2), pp 507–521.
[19] Zhang, J., Biggs, J.D., Ye, D. and Sun, Z. Extended-state-observer-based event-triggered orbit-attitude tracking for low-thrust spacecraft, *IEEE Trans. Aerosp. Electron. Syst.*, 2020, **56**, (4), pp 2872–2883.
[20] Di, F., Li, A., Guo, Y., Xie, C. and Wang, C. Event-triggered sliding mode attitude coordinated control for spacecraft formation flying system with disturbances, *Acta Astronaut.*, 2021, **188**, pp 121–129.
[21] Zhou, J., Wen, C. and Yang, G. Adaptive backstepping stabilization of nonlinear uncertain systems with quantized input signal, *IEEE Trans. Autom. Control*, 2014, **59**, (2), pp 460–464.
[22] Liu, Z., Wang, F., Zhang, Y. and Chen, C.L.P. Fuzzy adaptive quantized control for a class of stochastic nonlinear uncertain systems, *IEEE Trans. Cybern.*, 2016, **46**, (2), pp 524–534.
[23] Hu, Q. and Xiao, B. Intelligent proportional-derivative control for flexible spacecraft attitude stabilization with unknown input saturation, *Aerosp. Sci. Technol.*, 2012, **23**, (1), pp 63–74.
[24] An, H., Liu, J., Wang, C. and Wu, L. Approximate back-stepping fault-tolerant control of the flexible air-breathing hypersonic vehicle, *IEEE/ASME Trans. Mechatron.*, 2016, **21**, (3), pp 1680–1691.
[25] Di Mauro, G., Lawn, M. and Bevilacqua, R. Survey on guidance navigation and control requirements for spacecraft formation-flying missions, *J. Guid. Control Dyn.*, 2018, **41**, (3), pp 581–602.

https://doi.org/10.1017/aer.2023.23 Published online by Cambridge University Press

[26] Hu, Q., Shi, Y. and Shao, X. Adaptive fault-tolerant attitude control for satellite reorientation under input saturation, *Aerosp. Sci. Technol.*, 2018, **78**, pp 171–182.
[27] Polyakov, A. Nonlinear feedback design for fixed-time stabilization of linear control systems, *IEEE Trans. Autom. Control*, 2011, **57**, (8), pp 2106–2110.
[28] Zou, A. and Kumar, K.D. Finite-time attitude control for rigid spacecraft subject to actuator saturation, *Nonlinear Dyn.*, 2019, **96**, (2), pp 1017–1035.
[29] Yu, S., Yu, X., Shirinzadeh, B. and Man, Z. Continuous finite-time control for robotic manipulators with terminal sliding mode, *Automatica*, 2005, **41**, (11), pp 1957–1964.
[30] Qian, C. and Lin, W. A continuous feedback approach to global strong stabilization of nonlinear systems, *IEEE Trans. Autom. Control*, 2001, **46**, (7), pp 1061–1079.
[31] Tan, C., Yu, X. and Man, Z. Terminal sliding mode observers for a class of nonlinear systems, *Automatica*, 2010, **46**, (8), pp 1401–1404.
[32] Wu, J., Liu, K. and Han, D. Adaptive sliding mode control for six-dof relative motion of spacecraft with input constraint, *Acta Astronaut.*, 2013, **87**, pp 64–76.
[33] Ploen, S.R., Hadaegh, F.Y. and Scharf, D.P. Rigid body equations of motion for modeling and control of spacecraft formations. part 1: Absolute equations of motion. In *Proceedings of the 2004 American Control Conference*, volume 4, pages 3646–3653, 2004.
[34] Sinclair, A.J., Hurtado, J.E. and Junkins, J.L. Application of the cayley form to general spacecraft motion, *J. Guid. Control Dyn.*, 2006, **29**, (2), pp 368–373.
[35] Hong, Y., Hu, J. and Gao, L. Tracking control for multi-agent consensus with an active leader and variable topology, *Automatica*, 2006, **42**, (7), pp 1177–1182.
[36] Zhou, Z., Zhou, D., Shi, X., Li, R. and Kan, B. Prescribed performance fixed-time tracking control for a class of second-order nonlinear systems with disturbances and actuator saturation, *Int. J. Control*, 2021, **94**, (1), pp 223–234.
[37] Kun, Y.A.N., Mou, C.H.E.N., Qingxian, W.U. and Ronggang, Z.H.U. Robust adaptive compensation control for unmanned autonomous helicopter with input saturation and actuator faults, *Chinese J. Aeronaut.*, 2019, **32**, (10), pp 2299–2310.
[38] Shi, X., Zhou, Z., Zhou, D., Li, R. and Chen, X. Observer-based event-triggered fixed-time control for nonlinear system with full-state constraints and input saturation, *Int. J. Control*, 2022, **95**, (2), pp 432–446.
[39] Li, Y., Wang, C. and Wang, W. Adaptive quantized attitude control for spacecraft with input saturation. In *2017 13th IEEE International Conference on Control & Automation (ICCA)*, pages 449–454, 2017.
[40] Fan, R., Chen, X., Liu, M. and Cao, X. Attitude-orbit coupled sliding mode tracking control for spacecraft formation with event-triggered transmission, *ISA Trans.*, 2020, **6**, 338–348.
[41] Zhang, B. and Li, F. Adaptive finite-time control for six-degree-of-freedom leader-following spacecraft formation using twistors, *Adv. Space Res.*, 2022, **70**, (5), pp 1297–1311.

Cite this article: Zhang J., Xia H. and Li Z. (2023). Distributed fixed-time control for six-degree-of-freedom spacecraft formation with event-triggered observer. *The Aeronautical Journal*, **127**, 1968–1992. https://doi.org/10.1017/aer.2023.23